Accepted Manuscript

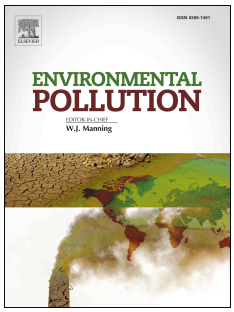

Redox and global interconnected proteome changes in mice exposed to complex environmental hazards surrounding Doñana National Park

Carmen Michán, Eduardo Chicano-Gálvez, Carlos A. Fuentes-Almagro, José Alhama

PII: S0269-7491(19)31103-0

DOI: https://doi.org/10.1016/j.envpol.2019.05.085

Reference: ENPO 12630

To appear in: *Environmental Pollution*

Received Date: 27 February 2019

Revised Date: 30 April 2019

Accepted Date: 16 May 2019

Please cite this article as: Michán, C., Chicano-Gálvez, E., Fuentes-Almagro, C.A., Alhama, José., Redox and global interconnected proteome changes in mice exposed to complex environmental hazards surrounding Doñana National Park, *Environmental Pollution* (2019), doi: https://doi.org/10.1016/j.envpol.2019.05.085.

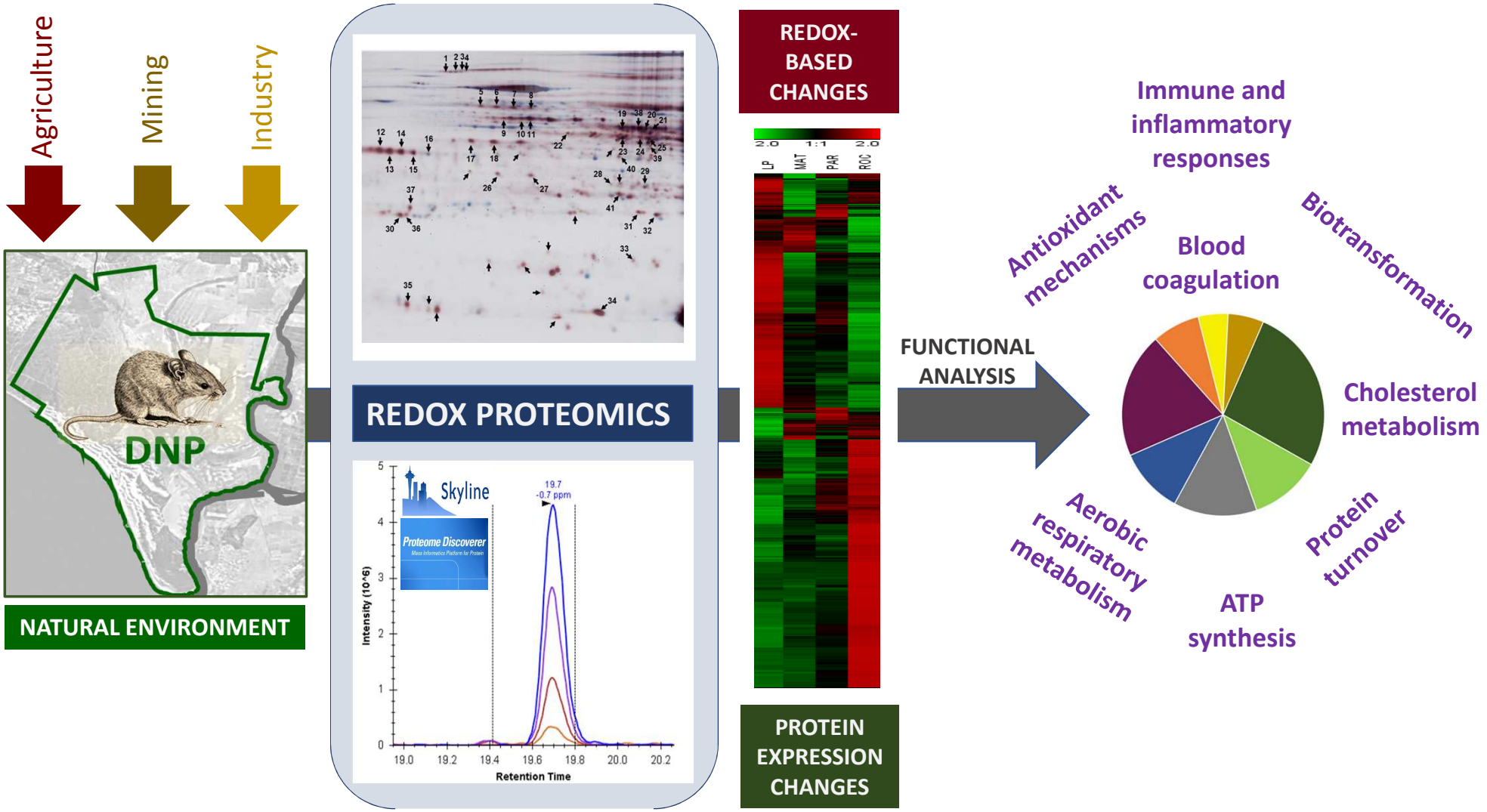
Agriculture
Mining
Industry
DNP
NATURAL ENVIRONMENT
REDOX PROTEOMICS
Skyline
Proteome Discoverer
19.7
-0.7 ppm
Intensity (10^6)
Retention Time
REDOX-BASED CHANGES
LP
MAT
PAR
ROC
PROTEIN EXPRESSION CHANGES
FUNCTIONAL ANALYSIS
Immune and inflammatory responses
Antioxidant mechanisms
Blood coagulation
Biotransformation
Cholesterol metabolism
Protein turnover
ATP synthesis
Aerobic respiratory metabolism

Redox and global interconnected proteome changes in mice exposed to complex environmental hazards surrounding Doñana National Park

Carmen Michán[a], Eduardo Chicano-Gálvez[a,b], Carlos A. Fuentes-Almagro[c], José Alhama[a,*]

[a] Department of Biochemistry and Molecular Biology, University of Córdoba, Córdoba, Spain

[b] Present address: Proteomics Unit, IMIBIC, Maimonides Institute for Biomedical Research, Córdoba, Spain

[c] Proteomics Unit, SCAI, University of Córdoba, Córdoba, Spain

* **Corresponding author:** Departamento de Bioquímica y Biología Molecular, Campus de Excelencia Internacional Agroalimentario CeiA3, Universidad de Córdoba, Campus de Rabanales, Edificio Severo Ochoa, E-14071 Córdoba, España.

E-mail address: bb2alcaj@uco.es (J. Alhama).

KEYWORDS:

Redox proteomics; label-free proteomics; pollutant-elicited oxidative stress; homeostasis; protein turnover

ABBREVIATIONS:

AhR, aryl hydrocarbon receptor; 2DE, two-dimensional electrophoresis; DNP, Doñana National Park; GO, Gene Ontology; 5-IAF, 5-iodoacetamidofluorescein; LC-MS/MS, liquid chromatography tandem mass spectrometry; LFQ, Label Free Quantification; LP, Lucio del Palacio; MAT, Matochal; MS, mass spectrometry; NEM, N-ethylmaleimide; PAR, Partido stream; RNS, reactive nitrogen species; ROC, Rocina stream; ROS, reactive oxygen species.

ABSTRACT

Natural environments are receiving an increasing number of contaminants. Therefore, the evaluation and identification of early responses to pollution in these complex habitats is an urgent and challenging task. Doñana National Park (DNP, SW Spain) has been widely used as a model area for environmental studies because, despite its strictly protected core, it is surrounded by numerous threat sources from agricultural, mining and industrial activities. Since many pollutants often induce oxidative stress, redox proteomics was used to detect redox-based variations within the proteome of *Mus spretus* mice captured in DNP and the surrounding areas. Functional analysis showed that most differentially oxidized proteins are involved in the maintenance of homeostasis, by eliciting mechanisms to respond to toxic substances and oxidative stress, such as antioxidant and biotransformation processes, immune and inflammatory responses, and blood coagulation. Furthermore, changes in the overall protein abundance were also analysed by label-free quantitative proteomics. The upregulation of phase I and II biotransformation enzymes in mice from Lucio del Palacio may be an alert for organic pollution in the area located at the heart of DNP. Metabolic processes involved in protein turnover (proteolysis, amino acid catabolism, new protein biosynthesis and folding) were activated in response to oxidative damage to these biomolecules. Consequently, aerobic respiratory metabolism increased to address the greater ATP demands. Alterations of cholesterol metabolism that could cause hepatic steatosis were also detected. The proteomic detection of globally altered metabolic and physiological processes offers a complete view of the main biological changes caused by environmental pollution in complex habitats.

CAPSULE: Redox proteomics in mice reveals interconnected biological responses to pollution near an environmentally protected area

1. Introduction

The extensive occurrence of pollution and its (ir)reversible damage to the ecosystems has become a common concern that requires urgent actions. The increasing release of contaminants may endanger the homeostasis of living-beings and threaten human health (Alhama Carmona et al., 2017; Pueyo et al., 2011). Frequently, environmental risk assessment is inferred from studies using acute exposure to one or a few toxins in laboratory-controlled experiments (Alhama et al., 2018; Morales-Prieto and Abril, 2017). However, in nature, organisms are usually exposed over long periods to multiple chemicals, which can also interact with each other and their effects may be affected by various biotic/abiotic factors. Chemical analysis, although useful in determining body-burdens, do not provide information about the biological effects of contaminants (López-Barea, 1995). Evaluating and identifying early responses to pollution in complex natural environments is an urgent and challenging task.

Doñana National Park (DNP) is a relevant wildlife reserve of great ecological value located in SW Spain. It is considered one of the most important natural protected areas in Europe. Furthermore, this location has been used as a model spot for environmental studies because it contains a presumably clean core site that has been strictly protected and is surrounded by areas that are exposed to numerous threats due to agricultural, mining and industrial undertakings (Abril et al., 2015; Abril et al., 2014; Abril et al., 2011; Bonilla-Valverde et al., 2004; Fernández-Cisnal et al., 2014; Fernandez-Cisnal et al., 2017; Garcia-Sevillano et al., 2014; García-Sevillano et al., 2012; Ruíz-Laguna et al., 2001; Ruiz-Laguna et al., 2016; Vioque-Fernández et al., 2009; Vioque-Fernández et al., 2007). Previous studies from our group have identified the presence of several pollutants threatening the area, such as prevailing metals and pesticides. Metals come mainly from the pyrite mines located in the north of the region and, to lesser extent, from the petrochemical and chemical industries near the city of Huelva (Abril et al., 2014; Garcia-Sevillano et al., 2014; García-Sevillano et al., 2012; Montes Nieto et al., 2010; Ruíz-Laguna et al., 2001; Ruiz-Laguna et al., 2016). In addition, pesticides are used extensively for rice, citrus and strawberry production in the nearby fields. Furthermore, agrochemical pollution in the region is considered particularly dangerous due to its intensive use and quick spread and to difficulties in its evaluation (Fernández-Cisnal et al., 2014; Gomara et al., 2008; Pueyo et al., 2011). Since the National Park is continuously threatened by pollution, a regular monitoring of the environment quality is required (García-Sevillano et al., 2012).

Mice are invaluable bioindicators of terrestrial pollution. Laboratory studies have traditionally used highly inbred *Mus musculus* lines with low levels of natural genetic

polymorphisms that may bias the obtained results (Dejager et al., 2009). Recently, other species of the *Mus* genus, such as *Mus spretus*, a.k.a. the Algerian mouse, are replacing *M. musculus*. The use of *M. spretus* as a bioindicator for pollution in Southern Europe and Northern Africa areas presents two main advantages. First, it presents low levels of inbreeding and thus has a larger amount of genetic variation. Second, *M. spretus* is not endangered and can be freely used for environmental pollution monitoring (Abril et al., 2015; Abril et al., 2014; Bonilla-Valverde et al., 2004; Dejager et al., 2009; Garcia-Sevillano et al., 2014; García-Sevillano et al., 2012; Montes-Nieto et al., 2007; Ruíz-Laguna et al., 2001; Ruiz-Laguna et al., 2016) as well as in-lab exposure experiments (Alhama et al., 2018; Morales-Prieto and Abril, 2017). In addition, *M. spretus* mice have a sedentary nature and territorial lifestyle, with daily displacements in the range of 27.8 to 112.0 m, which make them valuable local environmental bioindicators (Palomo et al., 2009).

Many pollutants (i.e., metals, pesticides, polycyclic aromatic hydrocarbons) may generate reactive O and N species (ROS/RNS) due to their redox cycling properties (Alhama et al., 2018; Braconi et al., 2011; Fernández-Cisnal et al., 2014; López-Barea, 1995; Morales-Prieto and Abril, 2017). ROS/RNS can alter all biomolecules, but proteins are particularly sensitive due to the presence of redox susceptible cysteines (Cys) (Ying et al., 2007). ROS-mediated posttranslational modifications play key roles in signalling during normal cell growth (Eaton, 2006; Tell, 2006; Ying et al., 2007), but when ROS levels increase, oxidative damage can cause serious harm or even death of the cell/organisms (Dalle-Donne et al., 2006; Davies, 2005; Eaton, 2006; Ying et al., 2007).

To assess environmental stress situations, conventional biomarkers have been extensively used. However, this approach has proven limited since it requires a deep knowledge of the toxicity mechanisms of pollutants and produces biased results due to the limited number of analyzed biomolecule, while excluding those whose relationship with contamination is still not known. Unlike the narrow and static classic biomarker approach, omics unbiased technologies monitor many biomolecules in a high-throughput manner, thus providing a global evaluation of the biological responses altered by exposure to contaminants in natural complex ecosystems (Abril et al., 2015; Alhama Carmona et al., 2017; García-Sevillano et al., 2014). Environmental proteomics provides a global view of the entire proteome in a biological system. This technique has become a very popular tool for the assessment of the biological impact of a contaminated site because it: (i) can reveal the biological pathways affected by the pollutant(s), (ii) identifies molecular biomarkers for the early detection of pollution, and (iii) does not need any previous knowledge of their toxicity mechanisms. Recently, attention has

119 focused not only on the protein levels but also on their Cys residues as they function as redox
120 sensors in cell signalling pathways and as early biomarkers for oxidative protein damage.
121 Redox proteomics can identify and quantify proteins, as well as inform us about the oxidation
122 state of their thiols (Eaton, 2006; Sheehan et al., 2010). Oxidative Cys modifications can be
123 detected by specifically labelling with fluorescent chemicals followed by 2-dimensional
124 electrophoresis (2DE) analysis. Furthermore, differentially oxidized spots can be identified by
125 mass spectrometry (MS) (Charles et al., 2014; Fernández-Cisnal et al., 2014; Perez et al., 2010).
126 Recently, a novel gel-free redox proteomic approach has been proposed (McDonagh et al.,
127 2014). This method differentially labels reduced and oxidized Cys with either light (d0) or
128 heavy (d5) forms of N-ethylmaleimide (NEM), respectively. Peptides can then be directly
129 identified, and their Cys oxidation status can be quantified by massive liquid chromatography-
130 tandem mass spectrometry (LC-MS/MS) (Alhama et al., 2018; McDonagh et al., 2014). The
131 application of redox proteomics to assess environmental problems is a field of growing
132 interest, since many pollutants toxicity occurs by eliciting oxidative stress (Alhama et al., 2018;
133 Alhama Carmona et al., 2017; Braconi et al., 2011; Fernández-Cisnal et al., 2014; Rainville et
134 al., 2015).

135 This work aimed to evaluate the biological responses of *M. spretus* mice, used as a
136 bioindicator, in a complex pollution-threatened and environmentally sensitive area, DNP, using
137 an integrated proteomic approach. First, redox proteomics using differential cysteine labelling
138 and two complementary analysis methods, 2DE and LC-MS/MS, allowed the detection of
139 redox-based variations within the proteome. Second, changes in the overall protein
140 abundance were also analysed by label-free quantitative proteomics. The detection of globally
141 altered metabolic and physiological processes offers us an image of the main biological targets
142 of environmental pollution and of the defensive responses to fight against pollutant-elicited
143 oxidative stress.

2. Materials and methods

2.1 Study areas, animal capture and tissue collection

M. spretus mice were captured from November to December 2009 at four sites in DNP and its surroundings (SW Spain, Fig. 1). Animals from the *Lucio del Palacio* (LP), due to its central location in the heart of DNP, have been habitually used as a reference, although previous studies have shown the presence of contaminants (García-Sevillano et al., 2012). The other three sites are nearby areas of intensive agriculture (Abril et al., 2015; Abril et al., 2011; Fernández-Cisnal et al., 2014; Fernandez-Cisnal et al., 2017; Garcia-Sevillano et al., 2014; García-Sevillano et al., 2012). *Matochal* (MAT) is affected by rice-growing fields and suffers the input of pesticides and metals used as algaecides in the growth of rice. The *Partido* (PAR) site is under the influence of citrus fruit and grape fields and several urban enclaves. In the upper part of the *Rocina* (ROC), the stream converges with several aquifers coming from large land extension covered with strawberry greenhouses. Mice were captured with live traps and transported alive to a nearby lab, where their gender and weight were determined before being sacrificed by cervical dislocation. Eight male mice per site were selected by their similar average weights (LP, 11.9 ± 0.8 g; MAT, 12.3 ± 1.3 g; PAR, 12.5 ± 0.6 g; ROC, 13.4 ± 0.6 g) for this study. Animals were dissected, livers were individually extracted and frozen in liquid N_2 and taken to the University of Córdoba, where they were kept frozen at -80°C. Each organ was individually pulverized under liquid N_2 in a SPEX SamplePrep 6770 Freezer/Mill (Metuchen, NJ, USA).

2.2 Labelling of oxidized protein thiols, two-dimensional electrophoresis, mass spectrometry and protein identification

To avoid interindividual variations, pools were prepared by mixing approximately 50 mg aliquots of frozen liver powder from each of eight male mice collected per site. For the labelling of oxidized thiols and 2DE separation, the same protocol as the one previously used to evaluate the level of protein oxidation in crayfish, from the same sampling sites in DNP and its surrounding areas, was followed (Fernández-Cisnal et al., 2014). Briefly, reversibly oxidized thiols in proteins were detected via alkylation/blocking of native thiols, cleavage of disulphide bonds and specific fluorescence labelling with 5-IAF of the newly reduced thiols. After labelling, proteins were separated by 2DE and fluorescence images of the gels were captured. The gels were also stained with SYPRO Ruby to reveal total proteins, used for normalization. To identify differentially oxidized proteins, spots were excised, tryptically digested and analysed by MS conducted in a MALDI-TOF/TOF. Proteins were identified through peptide mass

fingerprinting and confirmed through MS/MS analysis as previously described (Fernández-Cisnal et al., 2014), with taxonomy restriction to mouse (98 244 sequences when the Uniprot database was interrogated). The protein identifications were validated according to the following criteria: high score, sequence coverage, lowest expectation, number of matched peptides, and the number and score of the fragmented ions.

2.3 Label-based MS-based evaluation of the redox status of Cys-containing peptides

The reversible redox state of specific Cys residues in proteins was analysed using a high-throughput label-free quantitative proteomic approach, as previously described (Alhama et al., 2018). Briefly, after an initial differential labelling step of reduced and oxidized Cys residues with d(0)- and d(5)-NEM, respectively, protein samples were tryptically digested and analysed by LC-MS/MS. Raw data were processed using Proteome Discoverer and resulting MS2 spectra were searched using the SEQUEST engine against a database of UniProt Mus musculus_Feb2017 (www.uniprot.org). Finally, peptide identifications were grouped into proteins with Proteome Discoverer 2.1, and analysis of identified peptides was performed using Skyline software (http://proteome.gs.washington.edu/software/skyline) in MS1 filtering mode, as previously described (Alhama et al., 2018; Schilling et al., 2012).

Label-free quantification (LFQ) intensities were used to determine global levels of the proteins containing peptides with Cys residues, as previously described (Alhama et al., 2018).

2.4 Cluster analysis

The Genesis package (Sturn et al., 2002) was used for cluster analysis. Intensity data were normalized, and the distance measure employed was Pearson´s correlation. Complete linkage hierarchical clustering and k-means clustering analyses were performed.

2.5 Biological analysis of proteins

Biological interpretation of the list of proteins was first carried out using a Cytoscape plug-in, ClueGo (Bindea et al., 2009). By integrating Gene Ontology (GO) terms as well as KEGG/BioCarta pathways, a functionally organized GO/pathway term network was created. A list of proteins IDs was used to query the Gene Ontology-Biological Process database (European Bioinformatics Institute, EBI). ClueGo parameters were set as indicated: Go Term Fusion selected; only display pathways with p values ≤ 0.01; threshold of 10% of genes per pathway. Next, a molecular interaction network associated with input protein IDs was retrieved using BisoGenet, another Cytoscape plug-in (Martin et al., 2010). For both analyses, the *Mus musculus* database was used.

2.6 Statistical analysis

The 2DE data are presented as the mean ± SD of three independent gel images. They were analysed using GraphPad Instant software (version 3.05). The Student-Newman-Keuls multiple comparison test was calculated. A $p < 0.05$ was considered statistically significant.

3. Results

3.1 Fluorescence labelling of oxidized protein thiols and two-dimensional electrophoresis

Representative 2DE gel images of IAF-labelled oxidized thiol proteins (up, in red) and SYPRO Ruby-stained proteins (down, in blue) of mice from LP at the core of DNP are shown in Fig. 2A. The number of spots exhibiting reversibly oxidized thiols was 571 ± 290, which represents 47% of the 1206 ± 477 spots detected through SYPRO Ruby staining. The two previous representative images were aligned, as shown in Fig. 2B, which allowed us to determine the exact positions of the differentially oxidized thiol proteins in the SYPRO Ruby-stained gel for excision, tryptic digestion and analysis by MS. The arrows in Fig. 2B shows the positions of the selected 52 spots presenting differences in intensity (> 2-fold, $p < 0.05$) when the sampling sites were compared. The MS analysis using MALDI-TOF/TOF and genomic database searches resulted in the positive identification of 41 protein spots (79% of the total analysed proteins), which are numbered in Fig. 2B. Supplementary Table 1 shows the names of the identified proteins, some of the criteria used for validation of the identifications (Protein score, Expect and Sequence coverage) and the 5-IAF normalized intensities obtained at the different sampling sites. The 41 identified protein spots corresponded to 20 unique proteins, as a total of 10 proteins were identified from several spots. Thus, spots 1-4 were identified as TERA, 5-8 as SBP1, 9-11 as ENOA, 12-16 as RGN, 17-18 as F16P1, 19-21 as FAAA, 22-25 as ARGI1, 26-27 as NIT2, 28-29 as PGAM1 and spots 31-32 as PRDX1.

3.2 Differential isotopic cysteine labelling and mass spectrometry analysis

Although 2DE allows the evaluation of the levels of oxidation of proteins, it is a technology that is quite laborious and time-consuming. Therefore, with developments in MS technology, there is a growing trend to use higher sample throughput “gel-free” proteomics (Sheehan et al., 2010). Therefore, a massive LC-MS/MS analysis was applied to identify and quantify the reversible redox state of specific Cys residues in peptides after differential isotopic labelling of reduced/oxidized Cys residues with light (d0) and heavy (d5) forms of NEM, respectively. A total of 264 peptides, corresponding to 127 identified proteins, were present in the three replicates of the four sampling areas. Eighty proteins were considered in this study, including only those with peptides showing greater than 2-fold changes in the oxidation state of their Cys (p <0.05) when comparing sampling sites (Supplementary Table 2).

A hierarchical clustering analysis was carried out to visually quantify the alterations in the oxidation status of proteins (Fig. 3). The analysis included both the 41 differentially oxidized proteins resolved by 2DE and the peptides of the 80 proteins containing differentially oxidized cysteines quantified by LC-MS/MS. Proteins/peptides and sites were grouped into six clusters

based on similarities in their level of oxidation patterns. Half of the proteins, those grouped in clusters A (57) and B (24), correspond to proteins/peptides with more oxidation in LP. Fewer proteins/peptides, MAT (cluster C, 21), PAR (cluster D, 19) and ROC (cluster E, 23), had more oxidation at the other locations. Finally, cluster F included 18 proteins/peptides with a lower oxidation status at LP than all the other sampling sites. The cluster in which each protein/peptide is included is indicated in Supplementary Table 1 and Supplementary Table 2. Significantly, except for spots 15 and 32, included in cluster E, the rest of the protein spots separated by 2DE were part of cluster A, thus showing a higher level of oxidation at LP. In contrast, differentially oxidized Cys-containing peptides identified by LC-MS/MS were distributed throughout all the different clusters.

A Cytoscape analysis was carried out for the biological interpretation of the complete list of identified proteins. ClueGo was used to decipher functionally grouped proteins and to create a functionally organized GO/pathway term network (Fig. 4). This app identified four main functional GO groups; the top category was formed by proteins involved in “cell redox homeostasis and detoxification”, accounting for approximately 41% of the total proteins/peptides. Other groups were “immune and inflammatory response, and blood coagulation” (28.4%); “generation of precursor metabolites and energy” (18.5%); and “amino acid metabolic process” (12.3%). Table 1 lists the eighty-one differentially oxidized proteins (17 from the 2DE experiment and 64 from the LC-MS/MS experiment), and details how they are distributed and grouped into the four different functional GO groups. The oxidation pattern of the different protein spots/peptides is also specified. Of all the proteins, only GNMT and PRXD1 were identified in the two experiments, which indicates that these two techniques provide different information. It could be highlighted the high oxidation status of proteins involved in cell redox homeostasis and detoxification, including: CATA, GLRX5, HS90B, SBP1, PRDX2, PEBP1, PDIA6, RGN and TXND5 at LP (clusters A and B), CH60, CALR, ATOX1 and GLRX1 at MAT (cluster C), EST1 and MT1 at PAR (cluster D), and CERU, PDIA3 and THTR at ROC (cluster E).

Molecular interactions among the proteins identified from both proteomic approaches were studied using BisoGenet. Fig. 5 shows the network obtained in which a total of 58 proteins, 13 from the 2DE experiment and 45 from LC-MS/MS, are closely connected. Significantly, two proteins, EED (polycomb protein EED) and KCMA1 (calcium-activated potassium channel subunit alpha-1), occupy central nodes that connect many of the identified proteins.

3.3 Label-free quantitative proteomics analysis followed by a functional study

Changes in the overall protein abundance were analysed by label-free quantitative proteomics. A total of 1519 proteins were identified, of which 1177 were detected under all conditions. Of these, 720 proteins (~60%) showing ≥ 2-fold changes in any condition were considered in this study. A heatmap is presented to show the differential expression of proteins comparing mice from the different sites at DNP and its surroundings (Fig. 6). This analysis differentiates two patterns with a similar number of proteins. Cluster A grouped 328 proteins with higher intensity in LP and expression that decreased in mice from the other three areas, and cluster B was formed by proteins (392) with higher levels of expression at ROC (Fig. 6A). A ClueGo pathway analysis allowed us to assign functional groups to proteins from each of the two clusters (Fig. 6B and Supplementary Table 3). In cluster A, of the 76 proteins assigned to some metabolic pathways, approximately half are involved in the "metabolic transformation of drugs/xenobiotics", followed in proportion (22% of the total) by those involved in the "biosynthesis of cholesterol and subsequent metabolism of steroids". Approximately one-third of the proteins are involved in "proteolytic degradation in the proteasome" and subsequent "amino acid catabolism". The most numerous functional groups also include many enzymes involved in phase I metabolism (i.e., several cytochrome P450 isoenzymes, hydrolases, flavin monooxygenases) and phase II reactions (i.e., different UDP-glucuronosyltransferases and glutathione *S*-transferases). In cluster B, functional groups were assigned to 105 proteins, of which the highest percentage (62% of the total) corresponds to those involved in the processes of "translation and synthesis of proteins" (38%), their "processing and folding" (13%), and again their "proteolytic degradation in the proteasome" (10%). We would like to highlight the large number of protein-metabolism components identified (i.e., 40S and 60S ribosomal proteins, translation initiation factors, T-complex protein 1 subunits, proteasome structural and regulatory subunits). Additionally, a significant number of proteins (20%) participate in the response to oxidative stress and toxic substances. Somewhat lower is the number of mitochondrial proteins involved in fatty acid oxidation and metabolism of pyruvate and in being components of the electron transport chain as part of aerobic respiration and ATP synthesis.

4. Discussion

4.1 Redox proteomics

In this study, the redox status of thiol groups in proteins was analysed to assess the biological effects of contaminants in mice from Doñana National Park (DNP). Two different and complementary high-throughput proteomic approaches were implemented. First, after fluorescence labelling of reversibly oxidized Cys and 2DE separation, proteins with differences in reversibly oxidized thiol levels were evaluated. Second, a massive LC-MS/MS analysis was applied to identify and quantify the reversible redox state of specific Cys residues in peptides, after differential isotopic labelling of reduced/oxidized Cys residues.

Of the 41 differentially oxidized protein spots identified in the 2DE experiment (see Supplementary Table 1), only ten had unique identifications, since the other ten proteins were identified from several spots: TERA (4), SBP1 (4), ENOA (3), RGN (5), F16P1 (2), FAAA (3), ARGI1 (4), NIT2 (2), PGAM1 (2) and PRDX1 (2 spots). The different forms of the same protein have different pI values and slightly higher Mr values when shifted to a more acidic range, suggesting that they harbour different posttranslational modifications. LC-MS/MS analysis identified 127 proteins containing differentially oxidized Cys-containing peptides (Supplementary Table 2). Approximately half of the proteins (60) were identified containing only one Cys-oxidized peptide, and twenty proteins contained more than two peptides, highlighting serotransferrin and serum albumin containing 11 and 12 Cys-differentially oxidized peptides, respectively. Of all the proteins, only two were identified in both experiments, glycine N-methyltransferase (GNMT) and peroxiredoxin-1 (PRDX1), which indicates that these two techniques provide different information, although complementary, on the redox state of proteins. As shown above, 2DE evaluates the global oxidation level of proteins and reports about posttranslational modifications, while LC-MS/MS reports on the oxidation status of specific Cys in peptides. Significantly, two oxidized peptides were detected in PRDX1 (Supplementary Table 2), which could explain the two protein spots detected in the 2DE gel (spots 31 and 32; Fig. 2 and Supplementary Table 1).

Identified proteins showed different oxidation patterns, global or at specific Cys residues, indicating a complex metabolic response in mice that may be influenced by different biotic and abiotic factors. We would like to highlight anthropogenic activities carried out around DNP, mainly intensive agriculture and industries at Huelva Estuary, which currently represent an extremely serious threat to this unique biosphere reserve (Abril et al., 2015; Fernández-Cisnal et al., 2014; Fernandez-Cisnal et al., 2017; García-Sevillano et al., 2012). Globally, up to 50% of the proteins/peptides (81 from a total of 162) were included in clusters A and B (Fig. 3),

indicating a higher oxidation state of proteins in mice from LP at the core of DNP. Moreover, 95% of the differentially oxidized protein spots resolved by 2DE were included in cluster A, as shown in Supplementary Table 1. Some proteins contained several Cys residues with different reactivities. The most outstanding examples are ALBU and TRFE, proteins with 12 and 11 Cys-containing peptides, respectively, which present very different oxidation patterns (Table 1 and Supplementary Table 2), probably due to the influence of the residues located at the Cys nearby surroundings (Janssen-Heininger et al., 2008; Ying et al., 2007).

Functional analysis showed that most differentially oxidized proteins (approximately 40%) are involved in the maintenance of cellular redox homeostasis, by eliciting mechanisms to respond to toxic substances and to oxidative stress. Significantly, several of these proteins, including redoxins and related proteins (TXN, GLRX, PRDX, PDI), are characterized by having redox-active Cys residues. Here, TXND5, GLRX5, PRDX2 and PDIA6 presented higher oxidation at LP, while GLRX1 and PDIA3 were more oxidized at MAT and ROC, respectively. Thioredoxin (TXN), thioredoxin reductase and NADPH form the ubiquitous thioredoxin system. TXNs, with a dithiol-disulphide active site, act as antioxidants by facilitating the reduction of other proteins by cysteine thiol-disulfide exchange. This protein plays a role in many important biological processes, including redox signalling (Arner and Holmgren, 2000). Glutaredoxins (GLRX) utilize the reducing power of glutathione to catalyse disulphide reductions in the presence of NADPH and glutathione reductase, forming the glutaredoxin system. GLRX acts in antioxidant defence by reducing low-molecular-weight disulphides and proteins (as PRDX) (Fernandes and Holmgren, 2004). Similar to other redoxins, the cellular functions of GLRX are due to the wide range of redox potential associated with their active site -Cys-X-X-Cys- (Foloppe and Nilsson, 2004). Accordingly, changes in the oxidation status of the characteristic -CPYC- motif of GLRX1 were detected in response to pollution in this work. Peroxiredoxins (PRDX) are ubiquitous and relatively abundant proteins that play a role in cell protection against oxidative stress by reducing and detoxifying peroxides and as sensors of hydrogen peroxide-mediated signalling events (Wood et al., 2003). PRDX1 is a typical 2-Cys peroxiredoxin with a conserved loop-helix active site motif that contains a peroxidatic cysteine, identified as the molecular switch responsible for the redox-sensitive oligomerization of this protein (Wood et al., 2003). This conserved loop-helix motif (PLDFTFVCPTE) containing active Cys52, changed in the studied animals following pattern F (Table 1 and Supplementary Table 2). After reducing peroxides, PRDX requires the donation of electrons from reduced TXN to restore its catalytic activity (Rhee et al., 2001; Wood et al., 2003). Furthermore, protein disulphide isomerases (PDI) are thiol-disulphide oxidoreductases that contain a variable number of TXN domains. PDIs catalyse the formation and breakage of disulphide bonds between Cys residues within proteins as they

fold, thus allowing proteins to quickly find the correct arrangement of disulphide bonds in their fully folded state (Gruber et al., 2006).

The second major group of proteins with redox changes includes those involved in adaptive and innate immune responses, in the inflammatory response, and blood coagulation. These are also crucial processes for maintaining homeostasis. Activation of both the innate and acquired immune responses and induction of chronic inflammation was previously shown by heterologous microarray analysis of transcriptome alterations in mice living in a heavily polluted area (Abril et al., 2014; Ruiz-Laguna et al., 2016). When the innate immune system detects infection or tissue injury, it activates several signal transduction pathways that trigger protective inflammatory responses (Kawai and Akira, 2011; Lugrin et al., 2014; Newton and Dixit, 2012). However, increasing evidence indicates that excessive and/or chronic inflammation can result in tissue injury, organ dysfunction, different pathological processes and diseases, and cancer (Abril et al., 2014; Lugrin et al., 2014; Newton and Dixit, 2012). Moreover, oxidative stress plays a crucial role in the origin, development and perpetuation of inflammation and thus contributes to its pathological consequences (Lugrin et al., 2014). Blood coagulation, the immune system and inflammation maintain close communication that can either amplify or dampen the responses (Antoniak, 2017; Esmon, 2004; Xu et al., 2010). During infections, the blood coagulation system is activated, and components of the haemostatic system are directly involved in the immune response to limit pathogen dissemination (Antoniak, 2017). However, overactivation produces thrombotic complications, excessive inflammation, and tissue damage (Antoniak, 2017; Xu et al., 2010).

Many of the identified proteins are closely connected in a complex network of molecular interactions (Fig. 5). Significantly, two proteins, EED (polycomb protein EED) and KCMA1 (calcium-activated potassium channel subunit alpha-1), occupy central nodes that connect many of the differentially oxidized proteins and both are related to severe health problems. EED is a component of the polycomb repressive complex 2 (PRC2), a multiprotein chromatin-modifying complex that, by catalysing the mono-, di- and tri-methylation of histone H3 at lysine 27 and the transcriptional repression of the affected target genes, is essential for vertebrate development and differentiation (Conway et al., 2015; Ueda et al., 2016). Alteration of the level of this histone modification has been related to many types of cancer (Conway et al., 2015; Ezponda and Licht, 2014; Ueda et al., 2016). In contrast, potassium channels gated by calcium control different cellular processes in the liver, such as proliferation and volume homeostasis, showing a protective role during liver injury and fibrosis (Sevelsted Moller et al., 2016).

4.2 Label-free quantitative proteomics analysis

As previously described, differential isotopic labelling and MS analysis allowed us to evaluate the redox state of specific Cys-containing peptides in proteins. Additionally, this approach provides a set of raw data that can be used for the LFQ of the global levels of proteins, without the need for a further complete LC-MS/MS analysis. Globally, the deregulated proteins followed two quantitatively similar trends: those upregulated at LP and those showing higher intensity at ROC. Proteins responding to oxidative stress and toxic substances were clearly induced at ROC. A previous iTRAQ analysis showed that, compared with the LP reference, ROC mice proteins related to stress response presented higher changes than those from PAR and MAT animals (Abril et al., 2015). This area is affected by intense agricultural activity (strawberry, citrus fruit, and grape fields) and by diffuse pollution from petrochemical and chemical activities in its surroundings (García-Sevillano et al., 2012). LP, at the heart of DNP and within its area of maximum protection, has been widely considered as a reference/clean area (Abril et al., 2015; Fernández-Cisnal et al., 2014; Fernández-Cisnal et al., 2018; Vioque-Fernández et al., 2009). Our results show the upregulation of a high number of proteins involved in the biotransformation and metabolism of drugs/xenobiotics, which may be an early alert for organic pollution in the area. In this sense, the induction of up to 8 isoforms of the cytochrome P450 2 (CYP2) family suggests a remarkable response to drugs in mice from LP (Supplementary Table 3). Likewise, as discussed above, redox proteomics carried out here showed a higher oxidized status in proteins from LP mice. Serious suspicions about the absence of contamination in the centre of the Park have previously been reported, as unexpectedly high concentrations of metals (Cd, As, Mn, Cu and Zn) were found in LP mice. Furthermore, analysis of metals in soils and sediments from LP revealed higher concentrations of Cd and As than in those from PAR an ROC, and also unexpectedly high levels of Mn, Cu and Zn (García-Sevillano et al., 2012). The increasing responses of several biomarkers (G6PDH, SeGSHPx and EROD activities) at reference sites already attributed in 2001 to organic pollutants, such as pesticides used in intensive crops grown in areas nearby DNP, thus suggest the progressive pollution of key Doñana ecosystems (Bonilla-Valverde et al., 2004). Due to their sedentary lifestyle, it is unlikely that mice from contaminated areas around DNP would flow into LP (Palomo et al., 2009). In crayfish, although LP showed levels of biomarkers corresponding to a clean area, “Laguna Dulce”, also at the DNP core, had atypical levels in several pollution responsive biomarkers, which indicates that it is crucial to properly choose the reference area (Vioque-Fernández et al., 2009). To the presence of high metal levels already mentioned, there has been growing concern about the increasing presence of

448 emerging organic pollutants (i.e., human and veterinary pharmaceuticals, plasticizers,
449 surfactants) in aquatic organisms, wastewaters and surface waters at the surroundings of
450 Doñana (Camacho-Munoz et al., 2010; Garrido et al., 2016; Kazakova et al., 2018). The higher
451 number of upregulated proteins in mice from LP corresponds to phase I and II
452 biotransformation enzymes, which are involved in both adaptive and toxic effects of pollutants
453 (Abril et al., 2015). Many of these proteins are part of the aryl hydrocarbon receptor (AhR)
454 pathway, one of the most studied ligand-activated transcription factors, which functions as a
455 sensor of xenobiotic chemicals, especially aromatic hydrocarbons/dioxins (Michaelson et al.,
456 2011; Tian et al., 2015). Altogether, our results suggest the worrying presence of multiple
457 pollutants threaten this protected area.

458 Many pollutants generate ROS/RNS that induce oxidative stress (Braconi et al., 2011;
459 Fernández-Cisnal et al., 2014). A relevant negative consequence of stressing conditions is the
460 formation of oxidatively damaged (i.e., carbonylated, cross-linked or aggregated) proteins
461 (Braconi et al., 2011; Goldberg, 2003; Höhn et al., 2013; Wang et al., 2018). Approximately 80%
462 of proteins destined for degradation are labelled by ubiquitin in an energy-dependent process
463 and then digested by the 26S proteasome, which is a large proteolytic complex (Goldberg,
464 2003; Höhn et al., 2013; Jung and Grune, 2008; Laskowska et al., 2019). In this context, the
465 upregulation of components of the 26S proteasome system observed in this work could play
466 an important direct detoxification role by supporting the degradation of damaged proteins
467 under chronic pollutant exposure conditions (Elamin et al., 2016; Feng et al., 2018; Goldberg,
468 2003; Grune et al., 1997; Shimada et al., 2010; Wang et al., 2018). Because of their tendency to
469 form intracellular aggregates, misfolded or damaged proteins can be highly toxic and can
470 impair normal cellular functions, such as cell division, apoptosis or DNA damage repair, and
471 may lead to cell death and multiple pathologies (Davies and Shringarpure, 2006; Goldberg,
472 2003; Grune et al., 1997; Höhn et al., 2013; Laskowska et al., 2019). The 26S proteasome is
473 composed of a core 20S particle, in which proteins are digested to short peptides, and 1-2
474 regulatory particles, responsible for substrate recognition and transport into the core particle
475 (Díaz-Villanueva et al., 2015; Jung and Grune, 2008; Voges et al., 1999). Several components of
476 the 26S proteasome were upregulated at LP and ROC, including different subunits of the
477 catalytic core (20S proteasome), regulatory particles, and auxiliary proteins (ELOB, UBQL1,
478 UCHL3 and RS27A). LC-MS/MS redox proteomics showed a deubiquitinating enzyme (UBP19)
479 containing Cys248, which regulates the degradation of several proteins, to be highly oxidized
480 at LP (Table 1 and Supplementary Table 2) (Ogawa et al., 2011). After damaged-protein
481 degradation, the increased amino acid metabolism observed in LP can provide recycled
482 building blocks for the synthesis of new proteins (Höhn et al., 2013; Vabulas, 2007; Vellai and

Takács-Vellai, 2010). Changes in the redox status of Cys-containing proteins involved in amino acid metabolic processes are also reported here (Fig. 4 and Table 1). Under oxidative stress conditions, after removal of damaged proteins by effective proteolysis, the synthesis of new and protective proteins is vital to preserve cellular homeostasis, thus avoiding pathological situations (Dasuri et al., 2013). Significantly, many structural components of ribosome and translation factors were upregulated in mice from LP and ROC, which can be considered an adaptive response to stress (Vabulas, 2007). Thus, the synthesis of many protective proteins was clearly increased, including phase I and phase II biotransformation enzymes, antioxidant and auxiliary enzymes, and oxidative damage-repair enzymes. As happens with impaired proteolysis, reduced protein synthesis results in deleterious and toxic effects and contributes to disease pathogenesis (Caldarola et al., 2009; Dasuri et al., 2013).

The folding of newly synthesized proteins to their correct conformations is another critical process that requires the sequential actions of multiple molecular chaperones (Díaz-Villanueva et al., 2015; Goldberg, 2003). Up to 14 proteins involved in ensuring proper protein processing and chaperonin-mediated folding were upregulated in LP mice. Protein turnover within cells is a highly precise, selective and regulated global process, from its continuous degradation to amino acids and new protein synthesis to its subsequent proper folding (Díaz-Villanueva et al., 2015; Goldberg, 2003; Laskowska et al., 2019; Vellai and Takács-Vellai, 2010). It has been proposed that every step in the lifetime of proteins is safeguarded, with nearly all large subcellular mechanisms ready to react to proteotoxic stress (Díaz-Villanueva et al., 2015). These processes also demand a huge metabolic energy expenditure as it is estimated that protein degradation by the 26S proteasome uses approximately one-third of the ATP used by the ribosome in their synthesis (Voges et al., 1999). Otherwise, protein translation is the most energy-demanding process, accounting for ~75% of a cell´s total energy budget (Lane and Martin, 2010). To address the greater ATP demands, LP mice could respond with an increase in aerobic respiratory metabolism, based on the overexpression of proteins involved in fatty acid oxidation, in pyruvate metabolism and in the electron transport chain. Variations in the oxidation state of Cys-containing proteins involved in the generation of an energy precursor are shown in this work (Fig. 4 and Table 1).

Additionally, significant changes were detected in mitochondrial and peroxisomal proteins involved in fatty acid oxidation. Both organelles are key players in oxidative metabolism, showing close, coordinated and intricate metabolic and signalling cross-communication. Thus, dysfunction in one organelle exerts a direct negative effect on the other (Bonekamp et al., 2009; Fransen et al., 2012; Nordgren and Fransen, 2014). Although mitochondria have been mainly considered a major source of ROS, a precise and tightly regulated fine-tuning between

opposite pro-oxidant (*e.g.,* H_2O_2-generating oxidases) and antioxidant (especially catalase) mechanisms occurs in peroxisomes (Bonekamp et al., 2009; Fransen et al., 2012; Nordgren and Fransen, 2014). Peroxisome dysfunction has been linked to inherited and aged-related diseases and may play a role in the initiation and progression of oxidative stress-related diseases (Fransen et al., 2012; Nordgren and Fransen, 2014). Finally, peroxisomes act as sources of signalling messengers (specific lipids or different ROS/RNS) modulating various biological responses such as inflammatory responses, cytoprotective pathways, cell proliferation and differentiation, and senescence (Abril et al., 2015; Nordgren and Fransen, 2014).

Finally, cholesterol plays a vital role in animals, as it is an essential component of all cell membranes and it is a precursor of bile acid, vitamin D and especially steroid hormones, which control many physiological functions. Furthermore, cholesterol regulates ionic current mediated by the activity of Ca^{2+}-gated K^+ channels, thus controlling many physiological processes. Modification of channel function during hypercholesterolemia originates pathophysiological mechanisms leading to disease (Dopico et al., 2012). Alterations of cholesterol metabolism described in this work could be the origin of the accumulation of lipids in the liver (hepatic steatosis) previously described in *Mus spretus* mice living in a heavily polluted environment (Abril et al., 2014; Ruiz-Laguna et al., 2016). Additionally, oxidative stress has been related to the dysregulation of cholesterol metabolism via its role in the pathological progression of atherosclerosis (Kattoor et al., 2017; Morgan et al., 2016). Pollutant-associated activation of the AhR signalling pathway may contribute to the development of atherosclerosis through the induction of a vascular inflammatory response and accumulation of cholesterol (Tian et al., 2015; Wu et al., 2011) and to the development of steatohepatitis with fibrosis (Nault et al., 2017; Tian et al., 2015).

In conclusion, the holistic analysis of redox Cys status and total protein levels in mice captured near areas surrounding DNP show a complex pattern of changes that, although affecting very diverse metabolic pathways and physiological processes, seem to be molecularly interconnected. Alterations in functions such as "biotransformation metabolism of drugs/xenobiotics" or "maintenance of cell redox homeostasis" were expected, as some of the evaluated areas are heavily affected by pollution, and some of the previously detected pollutants generate oxidative stress. Our data also show that mouse health could be seriously compromised in the studied areas, as indicated by severe alterations in their immune responses/inflammatory response/blood coagulation, most likely due to pollutant-elicited tissue injury. Moreover, proteins are a primary target for oxidative damage. Increasing the metabolism of damaged or misfolded proteins, together with the concomitant biosynthesis of

553 new proteins, demands large quantities of energy, which will probably impair other metabolic
554 processes. Evaluating the response of an organism to complex environmental changes is not
555 an easy task. Only the combination of multiple proteomic approaches and the integration of
556 results will provide a complete picture of the real metabolic/physiological consequences.
557 Proteomics not only i) identifies proteins significantly altered after pollutant exposure, but also
558 informs about: ii) the types of contaminants present in complex ecosystems, iii) their toxic
559 mechanisms, and iv) the health status of exposed organisms. In this work, applying integrated
560 proteomics as a discovery-driven approach has alerted about the actual state of a highly
561 protected area, and suggests the need of further studies to determine contaminants and
562 sources of pollution.

563 **FIGURE LEGENDS**

564 Fig. 1. Map of Doñana National Park (DNP) and its surrounding areas showing the sites where
565 *Mus spretus* mice were captured. The locations of the sites in SW Spain and their UTM
566 coordinates are indicated.

567 Fig. 2. (A) Representative 2DE gel images of IAF-labelled oxidized thiol proteins (up) and SYPRO
568 Ruby-stained proteins (down) of *M. spretus* from LP. (B) An overlapping image of both gels is
569 also shown, in which the arrows mark the differentially oxidized thiol protein spots (> 2-fold
570 intensity differences, $p < 0.05$) when the sampling sites were compared. Numbers indicate the
571 proteins that were positively identified by MS, which are listed in Supplementary Table 1.

572 Fig. 3. K-means clustering analysis of the differentially oxidized proteins analysed by 2DE and
573 peptides identified by LC-MS/MS. Peptides/proteins are grouped into six clusters (A-F) for
574 which the trend is shown in the graphs on the left, indicating the number of peptides/proteins
575 of each cluster within the graph. Corresponding heatmaps are shown on the right of each
576 graph, in which each row represents one differentially oxidized peptide/protein. Green
577 rectangles indicate samples with lower oxidation levels relative to other conditions, while red
578 rectangles represent higher levels. The colour intensity is proportional to the fold-change as
579 represented by the scale.

580 Fig. 4. Functional groups obtained after GlueGo analysis of differentially oxidized proteins in
581 mice. The chart shows the four (GO 1-4) functional groups obtained after the analysis of the
582 total proteins identified by both techniques, 2DE and LC-MS/MS, and it represents the
583 percentage of terms per group.

584 Fig. 5. Molecular interactions network obtained using BisoGenet. The green circles refer to the
585 proteins identified in the 2DE experiment. The pink circles correspond to proteins from the LC-
586 MS/MS analysis. Light blue circles are proteins that, although not detected in this study,
587 functionally link the identified changing proteins.

588 Fig. 6. Analysis of the proteins quantified by label-free proteomics. (A) Hierarchical clustering
589 analysis of proteins showing ≥2-fold differential expression in at least one condition when
590 comparing mice from the different sites at DNP. Each row represents one differentially
591 expressed protein. Colour scale is row-normalised. Green rectangles indicate samples with
592 lower intensity relative to other conditions, while red rectangles represent higher intensity.
593 The colour intensity is proportional to the fold-change as represented by the scale. Proteins

are grouped into two clusters (A, B) for which the trend is shown in the graphs on the right, wherein the number of proteins comprising each cluster is indicated. (B) Overview charts with functional groups including differentially expressed proteins of clusters A (upper side) and B (lower side).

Acknowledgments

We would like to express our sincere thanks to Dr. Ricardo Fernández-Cisnal for technical assistance. The study was supported by the European Regional Development Fund, the Spanish Ministry of Economy and Competitiveness (MINECO, CTM2012-38720-C03-02 and CTM2015-67902-C2-1-P), the Agency of Economy, Competitiveness, Science, and Employment of the Andalusian Government (BIO1657) and by the Andalusian Plan of Research, Development, and Innovation (PAIDI) to group BIO187. The mass spectrometry analyses were carried out in the UCO-SCAI (Centralized Research Support Proteomic facility, University of Cordoba).

609 **REFERENCES**

610 **A**bril, N., Chicano-Gálvez, E., Michán, C., Pueyo, C., López-Barea, J., 2015. iTRAQ analysis of
611 hepatic proteins in free-living *Mus spretus* mice to assess the contamination status of areas
612 surrounding Donana National Park (SW Spain). Sci. Total Environ. 523, 16-27.

613 Abril, N., Ruiz-Laguna, J., Garcia-Sevillano, M.A., Mata, A.M., Gomez-Ariza, J.L., Pueyo, C., 2014.
614 Heterologous microarray analysis of transcriptome alterations in *Mus spretus* mice living in
615 an industrial settlement. Environ. Sci. Technol. 48, 2183-2192.

616 Abril, N., Ruiz-Laguna, J., Osuna-Jiménez, I., Vioque-Fernández, A., Fernández-Cisnal, R.,
617 Chicano-Gálvez, E., et al., 2011. Omic approaches in environmental issues. J. Toxicol.
618 Environ. Health A 74, 1001-1019.

619 Alhama Carmona, J., Michán Doña, C., López-Barea, J., 2017. New Trends in Aquatic Pollution
620 Monitoring: From Conventional Biomarkers to Environmental Proteomics. In: García
621 Barrera, Gómez Ariza (Eds.). Environmental Problems in Marine Biology: Methodological
622 Aspects and Applications. CRC Press, Boca Raton, pp. 150-171.

623 Alhama, J., Fuentes-Almagro, C.A., Abril, N., Michán, C., 2018. Alterations in oxidative
624 responses and post-translational modification caused by *p,p*-DDE in *Mus spretus* testes
625 reveal Cys oxidation status in proteins related to cell-redox homeostasis and male fertility.
626 Sci. Total Environ. 636, 656-669.

627 Antoniak, S., 2017. The coagulation system in host defense. Res. Pract. Thromb. Haemost. 2,
628 549-557.

629 Arner, E.S., Holmgren, A., 2000. Physiological functions of thioredoxin and thioredoxin
630 reductase. Eur. J. Biochem. 267, 6102-6109.

631 Braconi, D., Bernardini, G., Santucci, A., 2011. Linking protein oxidation to environmental
632 pollutants: Redox proteomic approaches. J. Proteomics 74, 2324-2337.

633 Bindea, G., Mlecnik, B., Hackl, H., Charoentong, P., Tosolini, M., Kirilovsky, A., et al., 2009.
634 ClueGO: a Cytoscape plug-in to decipher functionally grouped gene ontology and pathway
635 annotation networks. Bioinformatics 25, 1091-1093.

636 Bonekamp, N.A., Volkl, A., Fahimi, H.D., Schrader, M., 2009. Reactive oxygen species and
637 peroxisomes: struggling for balance. Biofactors 35, 346-355.

638 Bonilla-Valverde, D., Ruiz-Laguna, J., Muñoz, A., Ballesteros, J., Lorenzo, F., Gómez-Ariza, J.L., et
639 al., 2004. Evolution of biological effects of Aznalcollar mining spill in the Algerian mouse
640 (*Mus spretus*) using biochemical biomarkers. Toxicology 197, 123-138.

641 Braconi, D., Bernardini, G., Santucci, A., 2011. Linking protein oxidation to environmental
642 pollutants: Redox proteomic approaches. J. Proteomics 74, 2324-1337.

643 Caldarola, S., De Stefano, M.C., Amaldi, F., Loreni, F., 2009. Synthesis and function of ribosomal
644 proteins-fading models and new perspectives. Febs J. 276, 3199-3210.

645 Camacho-Muñoz, D., Martín. J., Santos, J.L., Aparicio, I., Alonso, E., 2010. Occurrence, temporal
646 evolution and risk assessment of pharmaceutically active compounds in Doñana Park
647 (Spain). J. Hazard Mater. 183, 602-608.

Conway, E., Healy, E., Bracken, A.P., 2015. PRC2 mediated H3K27 methylations in cellular identity and cancer. Curr. Opin. Cell Biol. 37, 42-48.

Charles, R., Jayawardhana, T., Eaton, P., 2014. Gel-based methods in redox proteomics. Biochim. Biophys. Acta 1840, 830-837.

Dalle-Donne, I., Scaloni, A., Butterfield, D.A., 2006. Redox Proteomics: From Protein Modifications to Cellular Dysfunction and Diseases. Hoboken, New Jersey, USA: John Wiley & Sons, Inc.

Dasuri, K., Zhang, L., Keller, J.N., 2013. Oxidative stress, neurodegeneration, and the balance of protein degradation and protein synthesis. Free Radic. Biol. Med. 62, 170-185.

Davies, K.J., Shringarpure, R., 2006. Preferential degradation of oxidized proteins by the 20S proteasome may be inhibited in aging and in inflammatory neuromuscular diseases. Neurology 66, S93-S96.

Davies, M.J., 2005. The oxidative environment and protein damage. Biochim. Biophys. Acta 1703, 93-109.

Dejager, L., Libert, C., Montagutelli, X., 2009. Thirty years of *Mus spretus*: a promising future. Trends Genet. 25, 234-241.

Díaz-Villanueva, J.F., Díaz-Molina, R., García-González, V., 2015. Protein folding and mechanisms of proteostasis. Int. J. Mol. Sci. 16, 17193-17230.

Dopico, A.M., Bukiya, A.N., Singh, A.K., 2012. Large conductance, calcium- and voltage-gated potassium (BK) channels: regulation by cholesterol. Pharmacol. Ther. 135, 133-150.

Eaton, P., 2006. Protein thiol oxidation in health and disease: techniques for measuring disulfides and related modifications in complex protein mixtures. Free Radic. Biol. Med. 40, 1889-1899.

Elamin, A., Titz, B., Dijon, S., Merg, C., Geertz, M., Schneider, T., et al., 2016. Quantitative proteomics analysis using 2D-PAGE to investigate the effects of cigarette smoke and aerosol of a prototypic modified risk tobacco product on the lung proteome in C57BL/6 mice. J. Proteomics 145, 237-245.

Esmon, C.T., 2004. Interactions between the innate immune and blood coagulation systems. Trends Immunol. 25, 536-542.

Ezponda, T., Licht, J.D., 2014. Molecular pathways: deregulation of histone H3 lysine 27 methylation in cancer-different paths, same destination. Clin. Cancer Res. 20, 5001-5008.

Feng, M., Yin, H., Peng, H., Lu, G., Liu, Z., Dang, Z., 2018. iTRAQ-based proteomic profiling of *Pycnoporus sanguineus* in response to co-existed tetrabromobisphenol A (TBBPA) and hexavalent chromium. Environ. Pollut. 242, 1758-1767.

Fernandes, A.P., Holmgren, A., 2004. Glutaredoxins: glutathione-dependent redox enzymes with functions far beyond a simple thioredoxin backup system. Antioxid. Redox Signal. 6, 63-74.

685 Fernández-Cisnal, R., Alhama, J., Abril, N., Pueyo, C., López-Barea, J., 2014. Redox proteomics
686 as biomarker for assessing the biological effects of contaminants in crayfish from Doñana
687 National Park. Sci. Total Environ. 490, 121-33.

688 Fernández-Cisnal, R., García-Sevillano, M.A., García-Barrera, T., Gómez-Ariza, J.L., Abril, N.,
689 2018. Metabolomic alterations and oxidative stress are associated with environmental
690 pollution in *Procambarus clarkii*. Aquat. Toxicol. 205, 76-88.

691 Fernandez-Cisnal, R., García-Sevillano, M.A., Gómez-Ariza, J.L., Pueyo, C., López-Barea, J., Abril,
692 N., 2017. 2D-DIGE as a proteomic biomarker discovery tool in environmental studies with
693 *Procambarus clarkii*. Sci. Total Environ. 584-585, 813-827.

694 Foloppe, N., Nilsson, L., 2004. The glutaredoxin -C-P-Y-C- motif: influence of peripheral
695 residues. Structure 12, 289-300.

696 Fransen, M., Nordgren, M., Wang, B., Apanasets, O., 2012. Role of peroxisomes in ROS/RNS-
697 metabolism: implications for human disease. Biochim. Biophys. Acta 1822, 1363-1373.

698 García-Sevillano, M.A., García-Barrera, T., Abril, N., Pueyo, C., López-Barea, J., Gómez-Ariza,
699 J.L., 2014. Omics technologies and their applications to evaluate metal toxicity in mice *M.*
700 *spretus* as a bioindicator. J. Proteomics 104, 4-23.

701 García-Sevillano, M.A., González-Fernández, M., Jara-Biedma, R., García-Barrera, T., López-
702 Barea, J., Pueyo, C., et al., 2012. Biological response of free-living mouse *Mus spretus* from
703 Doñana National Park under environmental stress based on assessment of metal-binding
704 biomolecules by SEC-ICP-MS. Anal. Bioanal. Chem. 404, 1967-1981.

705 Garrido, E., Camacho-Muñoz, D., Martín, J., Santos, A., Santos, J.L., Aparicio, I., et al., 2016.
706 Monitoring of emerging pollutants in Guadiamar River basin (South of Spain): analytical
707 method, spatial distribution and environmental risk assessment. Environ. Sci. Pollut. Res.
708 Int. 23, 25127-25144.

709 Goldberg, A.L., 2003. Protein degradation and protection against misfolded or damaged
710 proteins. Nature 426, 895-899.

711 Gomara, B., González, M.J., Baos, R., Hiraldo, F., Abad, E., Rivera, J., et al., 2008. Unexpected
712 high PCB and total DDT levels in the breeding population of red kite (*Milvus milvus*) from
713 Doñana National Park, south-western Spain. Environ. Int. 34, 73-78.

714 Gruber, C.W., Cemazar, M., Heras, B., Martin, J.L., Craik, D.J., 2006. Protein disulfide
715 isomerase: the structure of oxidative folding. Trends Biochem. Sci. 31, 455-64.

716 Grune, T., Reinheckel, T., Davies, K.J., 1997. Degradation of oxidized proteins in mammalian
717 cells. Faseb J. 11, 526-534.

718 Höhn, A., König, J., Grune, T., 2013. Protein oxidation in aging and the removal of oxidized
719 proteins. J. Proteomics 92, 132-159.

720 Janssen-Heininger, Y.M., Mossman, B.T., Heintz, N.H., Forman, H.J., Kalyanaraman, B., Finkel,
721 T., et al., 2008. Redox-based regulation of signal transduction: principles, pitfalls, and
722 promises. Free Radic. Biol. Med. 45, 1-17.

723 Jung, T., Grune, T., 2008. The proteasome and its role in the degradation of oxidized proteins.
724 IUBMB Life 60, 743-752.

725 Kattoor, A.J., Pothineni, N.V.K., Palagiri, D., Mehta, J.L., 2017. Oxidative Stress in
726 Atherosclerosis. Curr. Atheroscler. Rep. 19, 42.

727 Kazakova, J., Fernández-Torres, R., Ramos-Payán, M., Bello-López, M.A., 2018. Multiresidue
728 determination of 21 pharmaceuticals in crayfish (*Procambarus clarkii*) using enzymatic
729 microwave-assisted liquid extraction and ultrahigh-performance liquid chromatography-
730 triple quadrupole mass-spectrometry analysis. J. Pharm. Biomed. Anal. 160, 144-151.

731 Kawai, T., Akira, S., 2011. Regulation of innate immune signalling pathways by the tripartite
732 motif (TRIM) family proteins. EMBO Mol. Med. 3, 513-527.

733 Lane, N., Martin, W., 2010. The energetics of genome complexity. Nature 467, 929-934.

734 Laskowska, E., Kuczynska-Wisnik, D., Lipinska, B., 2019. Proteomic analysis of protein
735 homeostasis and aggregation. J. Proteomics. In press.

736 López-Barea, J., 1995. Biomarkers in ecotoxicology: an overview. In: Degen, Seiler, Bentely,
737 (Eds.). Toxicology in Transition. Springer, Berlin, pp. 57-79.

738 Lugrin, J., Rosenblatt-Velin, N., Parapanov, R., Liaudet, L., 2014. The role of oxidative stress
739 during inflammatory processes. Biol. Chem. 395, 203-230.

740 Martin, A., Ochagavia, M.E., Rabasa, L.C., Miranda, J., Fernandez-de-Cossio, J., Bringas, R.,
741 2010. BisoGenet: a new tool for gene network building, visualization and analysis. BMC
742 Bioinformatics 11, 91.

743 McDonagh, B., Sakellariou, G.K., Smith, N.T., Brownridge, P., Jackson, M.J., 2014. Differential
744 cysteine labeling and global label-free proteomics reveals an altered metabolic state in
745 skeletal muscle aging. J. Proteome Res. 13, 5008-5021.

746 Michaelson, J.J., Trump, S., Rudzok, S., Grabsch, C., Madureira, D.J., Dautel, F., et al., 2011.
747 Transcriptional signatures of regulatory and toxic responses to benzo-[a]-pyrene exposure.
748 BMC Genomics 12, 502.

749 Montes-Nieto, R., Fuentes-Almagro, C.A., Bonilla-Valverde, D., Prieto-Álamo, M.J., Jurado, J.,
750 Carrascal, M., et al., 2007. Proteomics in free-living *Mus spretus* to monitor terrestrial
751 ecosystems. Proteomics 7, 4376-4387.

752 Montes Nieto, R., García-Barrera, T., Gómez-Ariza, J.L., López-Barea, J., 2010. Environmental
753 monitoring of Domingo Rubio stream (Huelva Estuary, SW Spain) by combining
754 conventional biomarkers and proteomic analysis in *Carcinus maenas*. Environ. Pollut. 158,
755 401-408.

756 Morales-Prieto, N., Abril, N., 2017. REDOX proteomics reveals energy metabolism alterations in
757 the liver of *M. spretus* mice exposed to *p,p'*-DDE. Chemosphere 186, 848-863.

758 Morgan, A.E., Mooney, K.M., Wilkinson, S.J., Pickles, N.A., Mc Auley, M.T., 2016. Cholesterol
759 metabolism: A review of how ageing disrupts the biological mechanisms responsible for its
760 regulation. Ageing Res. Rev. 27, 108-124.

761 Nault, R., Fader, K.A., Lydic, T.A., Zacharewski, T.R., 2017. Lipidomic Evaluation of Aryl
762 Hydrocarbon Receptor-Mediated Hepatic Steatosis in Male and Female Mice Elicited by
763 2,3,7,8-Tetrachlorodibenzo-*p*-dioxin. Chem. Res. Toxicol. 30, 1060-1075.

764 Newton, K., Dixit, V.M., 2012. Signaling in innate immunity and inflammation. Cold Spring
765 Harb. Perspect. Biol. 4, a006049.

766 Nordgren, M., Fransen, M., 2014. Peroxisomal metabolism and oxidative stress. Biochimie 98,
767 56-62.

768 Ogawa, M., Yamaji, R., Higashimura, Y., Harada, N., Ashida, H., Nakano, Y., et al., 2011. 17beta-
769 estradiol represses myogenic differentiation by increasing ubiquitin-specific peptidase 19
770 through estrogen receptor alpha. J. Biol. Chem. 286, 41455-41465.

771 Palomo, L.J., Justo, E.R., Vargas, J.M., 2009. *Mus spretus* (Rodentia: Muridae). Mamm. Species
772 840, 1-10.

773 Pérez, V.I., Pierce, A., de Waal, E.M., Ward, W.F., Bokov, A., Chaudhuri, A., et al., 2010.
774 Detection and quantification of protein disulfides in biological tissues a fluorescence-based
775 proteomic approach. Methods Enzymol. 473, 161-177.

776 Pueyo, C., Gómez-Ariza, J.L., Bello-López, M.A., Fernández-Torres, R., Abril, N., Alhama, J., et
777 al., 2011. New methodologies for assessing the presence and ecological effects of pesticides
778 in Doñana National Park (SW Spain). In: Sotytcheva (Ed.). Pesticides in the Modern World -
779 Trends in Pesticides Analysis. INTECH open, Rijeka, Croatia, pp. 165-196.

780 Rainville, L.C., Coelho, A.V., Sheehan, D., 2015. Application of redox-proteomics tool-box to
781 *Daphnia magna* challenged with model pro-oxidants copper and paraquat. Environ. Toxicol.
782 Chem. 34, 84-91.

783 Rhee, S.G., Kang, S.W., Chang, T.S., Jeong, W., Kim, K., 2001. Peroxiredoxin, a novel family of
784 peroxidases. IUBMB Life 52, 35-41.

785 Ruiz-Laguna, J., García-Alfonso, C., Peinado, J., Moreno, S., Ieradi, L.A., Cristaldi, M., et al.,
786 2001. Biochemical biomarkers of pollution in Algerian mouse (*Mus spretus*) to assess the
787 effects of the Aznalcollar disaster on Doñana Park (Spain). Biomarkers 6, 146-160.

788 Ruiz-Laguna, J., Vélez, J.M., Pueyo, C., Abril, N., 2016. Global gene expression profiling using
789 heterologous DNA microarrays to analyze alterations in the transcriptome of *Mus spretus*
790 mice living in a heavily polluted environment. Environ. Sci. Pollut. Res. Int. 23, 5853-5867.

791 Schilling, B., Rardin, M.J., MacLean, B.X., Zawadzka, A.M., Frewen, B.E., Cusack, M.P., et al.,
792 2012. Platform-independent and label-free quantitation of proteomic data using MS1
793 extracted ion chromatograms in skyline: application to protein acetylation and
794 phosphorylation. Mol. Cell. Proteomics 11, 202-214.

795 Sevelsted Moller, L., Fialla, A.D., Schierwagen, R., Biagini, M., Liedtke, C., Laleman, W., et al.,
796 2016. The calcium-activated potassium channel KCa3.1 is an important modulator of
797 hepatic injury. Sci. Rep. 6, 28770.

798 Sheehan, D., McDonagh, B., Bárcena, J.A., 2010. Redox proteomics. Expert. Rev. Proteomics 7,
799 1-4.

800 Shimada, M., Kameo, S., Sugawara, N., Yaginuma-Sakurai, K., Kurokawa, N., Mizukami-Murata,
801 S., et al., 2010. Gene expression profiles in the brain of the neonate mouse perinatally
802 exposed to methylmercury and/or polychlorinated biphenyls. Arch. Toxicol. 84, 271-286.

803 Sturn, A., Quackenbush, J., Trajanoski, Z., 2002. Genesis: cluster analysis of microarray data.
804 Bioinformatics 18, 207-8.

805 Tell, G., 2006. Early molecular events during response to oxidative stress in human cells by
806 differential proteomics. In: Dalle-Donne, Scaloni, Butterfield (Eds.). Redox Proteomics: From
807 Protein Modifications to Cellular Dysfunction and Diseases. John Wiley & Sons, Inc.,
808 Hoboken, New Jersey, USA, pp. 369-397.

809 Tian, J., Feng, Y., Fu, H., Xie, H.Q., Jiang, J.X., Zhao, B., 2015. The aryl hydrocarbon receptor: a
810 key bridging molecule of external and internal chemical signals. Environ. Sci. Technol. 49,
811 9518-9531.

812 Ueda, T., Nakata, Y., Nagamachi, A., Yamasaki, N., Kanai, A., Sera, Y., et al., 2016. Propagation
813 of trimethylated H3K27 regulated by polycomb protein EED is required for embryogenesis,
814 hematopoietic maintenance, and tumor suppression. Proc. Natl. Acad. Sci. U.S.A. 113,
815 10370-10375.

816 Vabulas, R.M., 2007. Proteasome function and protein biosynthesis. Curr. Opin. Clin. Nutr.
817 Metab. Care 10, 24-31.

818 Vellai, T., Takács-Vellai, K., 2010. Regulation of protein turnover by longevity pathways. Adv.
819 Exp. Med. Biol. 694, 69-80.

820 Vioque-Fernández, A., Alves de Almeida, E., López-Barea, J., 2009. Assessment of Doñana
821 National Park contamination in *Procambarus clarkii*: integration of conventional biomarkers
822 and proteomic approaches. Sci. Total Environ. 407, 1784-1797.

823 Vioque-Fernández, A., de Almeida, E.A., Ballesteros, J., García-Barrera, T., Gómez-Ariza, J.L.,
824 López-Barea, J., 2007. Doñana National Park survey using crayfish (*Procambarus clarki*i) as
825 bioindicator: esterase inhibition and pollutant levels. Toxicol. Lett. 168, 260-268.

826 Voges, D., Zwickl, P., Baumeister, W., 1999. The 26S proteasome: a molecular machine
827 designed for controlled proteolysis. Annu. Rev. Biochem. 68, 1015-1068.

828 Wang, C., Rong, H., Liu, H., Wang, X., Gao, Y., Deng, R., et al., 2018. Detoxification mechanisms,
829 defense responses, and toxicity threshold in the earthworm *Eisenia foetida* exposed to
830 ciprofloxacin-polluted soils. Sci. Total Environ. 612, 442-449.

831 Wood, Z.A., Schroder, E., Robin Harris, J., Poole, L.B., 2003. Structure, mechanism and
832 regulation of peroxiredoxins. Trends Biochem. Sci. 28, 32-40.

833 Wu, D., Nishimura, N., Kuo, V., Fiehn, O., Shahbaz, S., Van Winkle, L., et al., 2011. Activation of
834 aryl hydrocarbon receptor induces vascular inflammation and promotes atherosclerosis in
835 apolipoprotein E-/- mice. Arterioscler. Thromb. Vasc. Biol. 31, 1260-1267.

836 Xu, J., Lupu, F., Esmon, C.T., 2010. Inflammation, innate immunity and blood coagulation.
837 Hamostaseologie 30, 5-6, 8-9.

838 Ying, J., Clavreul, N., Sethuraman, M., Adachi, T., Cohen, R.A., 2007. Thiol oxidation in signaling
839 and response to stress: detection and quantification of physiological and pathophysiological
840 thiol modifications. Free Radic. Biol. Med. 43, 1099-1108.
841
842

Table 1: List of proteins differentially oxidized in mice from DNP, distributed and grouped by GO functional groups.

Accession[a]	Protein Name (abbreviation)[a]	Experiment[b]	Protein spot no. or Peptide[c]	Cluster[d]
1. Cell redox homeostasis and detoxification (response to toxic substances and to oxidative stress)				
P63101	14-3-3 protein zeta/delta (1433Z)	LC-MS/MS	DICNDVLSLLEK	C
P63038	60 kDa heat shock protein. Mitochondrial (CH60)	LC-MS/MS	CEFQDAYVLLSEKK	C
P50247	Adenosylhomocysteinase (SAHH)	2DE	38	A
P14211	Calreticulin (CALR)	LC-MS/MS	DMHGDSEYNIMFGPDICGPGTKK	C
Q8C196	Carbamoyl-phosphate synthase [ammonia]. Mitochondrial (CPSM)	LC-MS/MS	SAYALGGLGSGICPNK - CEMASTGEVACFGEGIHTAFLK	B - F
Q8VCT4	Carboxylesterase 1D (CES1D)	LC-MS/MS	ENIPLQFSEDCLYLNIYTPADLTK - KENIPLQFSEDCLYLNIYTPADLTK - AISESGVSLTAALITTDVKPIAGLVATLSGCK	B - D - D
P24270	Catalase (CATA)	LC-MS/MS	LVNADGEAVYCK	A
Q61147	Ceruloplasmin (CERU)	LC-MS/MS	EMGPTYADPVCLSK	E
O08997	Copper transport protein ATOX1 (ATOX1)	LC-MS/MS	VCIDSEHSSDTLLATLNK	C
P58252	Elongation factor 2 (EF2)	LC-MS/MS	DLEEDHACIPIKK	B
Q01279	Epidermal growth factor receptor (EGFR)	LC-MS/MS	NYVVTDHGSCVR	D
Q9QUH0	Glutaredoxin-1 (GLRX1)	LC-MS/MS	VVVFIKPTCPYCR	C
Q80Y14	Glutaredoxin-related protein 5 (GLRX5)	2DE	35	A
P11499	Heat shock protein HSP 90-beta (HS90B)	LC-MS/MS	CLELFSELAEDKENYKK	B
Q8VCC2	Liver carboxylesterase 1 (EST1)	LC-MS/MS	TTTSAAMVHCLR	D
P02802	Metallothionein-1 (MT1)	LC-MS/MS	GAADKCTCCA	D
Q8VCC2	Methanethiol oxidase (SBP1)	2DE	5 - 6 - 7 - 8	A - A - A - A
O08601	Microsomal triglyceride transfer protein large subunit (MTP)	LC-MS/MS	ALDTCKIER	B
P35700	Peroxiredoxin-1 (PRDX1)	2DE	31 - 32	A - E
P35700	Peroxiredoxin-1 (PRDX1)	LC-MS/MS	GKYVVFFFYPLDFTFVCPTEIIAFSDR - HGEVCPAGWKPGSDTIKPDVNK	F - F
Q61171	Peroxiredoxin-2 (PRDX2)	2DE	30	A
P99029	Peroxiredoxin-5. Mitocondrial (PRDX5)	LC-MS/MS	ALNVEPDGTGLTCSLAPNILSQL - GVLFGVPGAFTPGCSK	C - F
P70296	Phosphatidylethanolamine-binding protein 1 (PEBP1)	2DE	36	A
P27773	Protein disulfide-isomerase A3 (PDIA3)	LC-MS/MS	VDCTANTNTCNK	E
Q922R8	Protein disulfide-isomerase A6 (PDIA6)	LC-MS/MS	TCEEHQLCVVAVLPHILDTGAAGR	B
Q64374	Regucalcin (RGN)	2DE	12 - 13 - 14 - 16 - 15	A - A - A - A - E
Q64105	Sepiapterin reductase (SPRE)	2DE	41	A
Q921I1	Serotransferrin (TRFE)	LC-MS/MS	WCAVSEHENTK - KTSYPDCIK - AVSSFFSGSCVPCADPVAFPK - CLKDGGGDVAFVK - DQYELLCLDNTR NQQEGVCPEGSIDNSPVK - SCHTGVDR - NLKQEDFELLCPDGTR - NLKQEDFELLCPDGTRKPVK KPVKDFASCHLAQAPNHVVVSR - DFASCHLAQAPNHVVVSR	E - E - E - D - E B - A - D - B D - E
P07724	Serum albumin (ALBU)	LC-MS/MS	TCVADESAANCDK - QEPERNECFLQHK - NECFLQHK - MKCSSMQK - ECCHGDLLECADDR ECCHGDLLECADDRAELAK - LQTCCDKPLLKK - CCAEANPPACYGTVLAEFQPLVEEPK – CCSGSLVER RPCFSALTVDETYVPK -EFKAETFTFHSDICTLPEK - AETFTFHSDICTLPEKEK	A - A - B - E - F D - B - F - E A - C - F
P10639	Thioredoxin (THIO)	LC-MS/MS	CMPTFQFYK	F

Q91W90	Thioredoxin domain-containing protein 5 (TXND5)	LC-MS/MS	IGKVDCTQHYAVCSEHQVR	B
P52196	Thiosulfate sulfurtransferase (THTR)	LC-MS/MS	KVDLSQPLIATCR	E
Q3UJD6	Ubiquitin carboxyl-terminal hydrolase 19 (UBP19)	LC-MS/MS	LCAPPMNTQTSLLSSEK	A
2.	***Immune and inflammatory response, and blood coagulation***			
P63260	Actin. cytoplasmic 2 (ACTG)	LC-MS/MS	CPEALFQPSFLGMESCGIHETTFNSIMK	E
P29699	Alpha-2-HS-glycoprotein (FETUA)	LC-MS/MS	ELACDDPEAEQVALLAVDYLNNHLLQGFK - QLTEHAVEGDCDFHILK - AQNVPLPVSTLVEFVIAATDCTAK	A - B - B
P32261	Antithrombin-III (ANT3)	LC-MS/MS	DIPVNPLCIYR	F
Q61176	Arginase-1 (ARGI1)	2DE	22 - 23 - 24 - 25	A - A - A - A
P10605	Cathepsin B (CATB)	LC-MS/MS	EQWSNCPTIGQIR - SCEAGYSPSYKEDK	E- E
P18242	Cathepsin D (CATD)	LC-MS/MS	GGCEAIVDTGTSLLVGPVEEVK	B
P01027	Complement C3 (CO3)	LC-MS/MS	VELLHNPAFCSMATAK	A
Q3ULW5	Ferritin (Q3ULW5)	LC-MS/MS	ADPHLCDFLESHFLDK - ADPHLCDFLESHFLDKEVK	A - A
P09528	Ferritin heavy chain (FRIH)	LC-MS/MS	LATDKNDPHLCDFIETYYLSEQVK	A
Q8K0E8	Fibrinogen beta chain (FIBB)	LC-MS/MS	CHAANPNGR - VYCDMK	C - E
Q8VCM7	Fibrinogen gamma chain (FIBG)	LC-MS/MS	DCQEIANKGAK - CHAGHLNGVYHQGGTYSK	A - B
P11276	Fibronectin (FINC)	LC-MS/MS	FGFCPMAAHEEICTTNEGVMYR	B
Q61646	Haptoglobin (HPT)	LC-MS/MS	QWVNTVAGEKLPECEAVCGKPK	D
P02089	Hemoglobin subunit beta-2 (HBB2)	LC-MS/MS	GTFASLSELHCDK	E
Q91X72	Hemopexin (HEMO)	LC-MS/MS	CSPDPGLTALLSDHR - GECQSEGVLFFQGNRK	B - E
Q9ESB3	Histidine-rich glycoprotein (HRG)	LC-MS/MS	AQDDCLPSR	C
P01868	Ig gamma-1 chain C region secreted form (IGHG1)	LC-MS/MS	TTPPSVYPLAPGSAAQTNSMVTLGCLVK	E
P01865	Ig gamma-2A chain C region. membrane-bound form (GCAM)	LC-MS/MS	TTAPSVYPLAPVCGDTTGSSVTLGCLVK	F
P01867	Ig gamma-2B chain C region (IGG2B)	LC-MS/MS	CPAPNLEGGPSVFIFPPNIKDVLMISLTPK	D
P01837	Ig kappa chain C region (IGKC)	LC-MS/MS	HNSYTCEATHK	A
P20918	Plasminogen (PLMN)	LC-MS/MS	KLYDYCDIPLCASASSFECGKPQVEPK	C
O70570	Polymeric immunoglobulin receptor (PIGR)	LC-MS/MS	GCHILPSHDEGAR	A
P21614	Vitamin D-binding protein (VTDB)	LC-MS/MS	SCESDAPFPVHPGTPECCTK	F
3.	***Generation of precursor metabolites and energy***			
Q99KI0	Aconitate hydratase. Mitocondrial (ACON)	LC-MS/MS	DVGGIVLANACGPCIGQWDR	B
P17182	Alpha-enolase (ENOA)	2DE	9 - 10 - 11	A - A - A
P99028	Cytochrome b-c1 complex subunit 6. Mitochondrial (QCR6)	LC-MS/MS	SQTEEDCTEELFDFLHAR - DHCVAHK	F - F
Q8R0Y6	Cytosolic 10-formyltetrahydrofolate dehydrogenase (AL1L1)	LC-MS/MS	GENCIAAGR	C
O08749	Dihydrolipoyl dehydrogenase. Mitocondrial (DLDH)	LC-MS/MS	VCHAHPTLSEAFR	E
Q91Y97	Fructose-bisphosphate aldolase B (ALDOB)	LC-MS/MS	IADQCPSSLAIQENANALAR	D
Q9QXD6	Fructose-1,6-biphosphatase 1 (F16P1)	2DE	17 -18	A - A
P16858	Glyceraldehyde-3-phosphate dehydrogenase (G3P)	LC-MS/MS	IVSNASCTTNCLAPLAK	B

Q3ULJ0	Glycerol-3-phosphate dehydrogenase 1-like protein (GPD1L)	LC-MS/MS	MAAAPLKVCIVGSGNWGSAVAK	A
P06151	L-lactate dehydrogenase A chain (LDHA)	LC-MS/MS	IVSSKDYCVTANSK - IVSSKDYCVTANSKLVIITAGAR - DYCVTANSK	C - F - F
Q9CPU0	Lactoylglutathione lyase (LGUL)	2DE	37	A
P08249	Malate dehydrogenase. Mitocondrial (MDHM)	LC-MS/MS	GCDVVVIPAGVPR	B
Q9DBJ1	Phosphoglycerate mutase 1 (PGAM1)	2DE	28 - 19	A - A
P09411	Phosphoglycerate kinase 1 (PGK1)	LC-MS/MS	GCITIIGGGDTATCCAK	C
Q01853	Transitional endoplasmic reticulum ATPase (TERA)	2DE	1 - 2 - 3 - 4	A - A - A - A
4.	***Amino acid metabolic process***			
Q91YI0	Argininosuccinate lyase (ARLY)	LC-MS/MS	DFVAEFLFWASLCMTHLSR - CAGLLMTLK	A - C
P05202	Aspartate aminotransferase. Mitochondrial (AATM)	LC-MS/MS	VGAFTVVCK	B
O35490	Betaine--homocysteine S-methyltransferase 1 (BHMT1)	LC-MS/MS	ASGKPVAATMCIGPEGDLHGVPPGECAVR - VNEAACDIAR	C - F
Q8C196	Carbamoyl-phosphate synthase [ammonia]. Mitochondrial (CPSM)	LC-MS/MS	SAYALGGLGSGICPNK - CEMASTGEVACFGEGIHTAFLK	B - F
P35505	Fumarylacetoacetase (FAAA)	2DE	19 - 20 - 21	A - A - A
P35492	Histidine ammonia-lyase (HUTH)	LC-MS/MS	EGLALINGTQMITSLGCEALER - ALCHPSSVDSLSTSAATEDHVSMGGWAAR	C - C
Q9QXF8	Glycine N-methylatransferase (GNMT)	2DE	40	A
Q9QXF8	Glycine N-methylatransferase (GNMT)	LC-MS/MS	VLDVACGTGVDSIMLVEEGFSVMSVDASDK	D
Q9JHW2	Omega-amidase NIT2 (NIT2)	2DE	26 - 27	A - A
Q91X83	S-adenosylmethionine synthase isoform type-1 (METK1)	LC-MS/MS	TCNVLVALEQQSPDIAQCVHLDR	C

[a] Protein name, abbreviation and accession obtained from UniProtKB/Swiss-Prot database.
[b] Differentially oxidized proteins resolved by 2DE and identified by MALDI-TOF/TOF analysis (2DE) and proteins containing peptides that showed changes in the oxidation state of their Cys identified differential isotopic labelling and mass spectrometry analysis (LC-MS/MS).
[c] Proteins spots numbers correspond to those resolved by 2DE (Fig. 2) and which are listed in Supplementary Table 1. Peptides identified by LC-MS/MS, as shown in Supplementary Table 3.
[d] Cluster name, corresponding to the different protein spots/peptides, given by Genesis analysis as shown in Fig. 3.

Figure 1

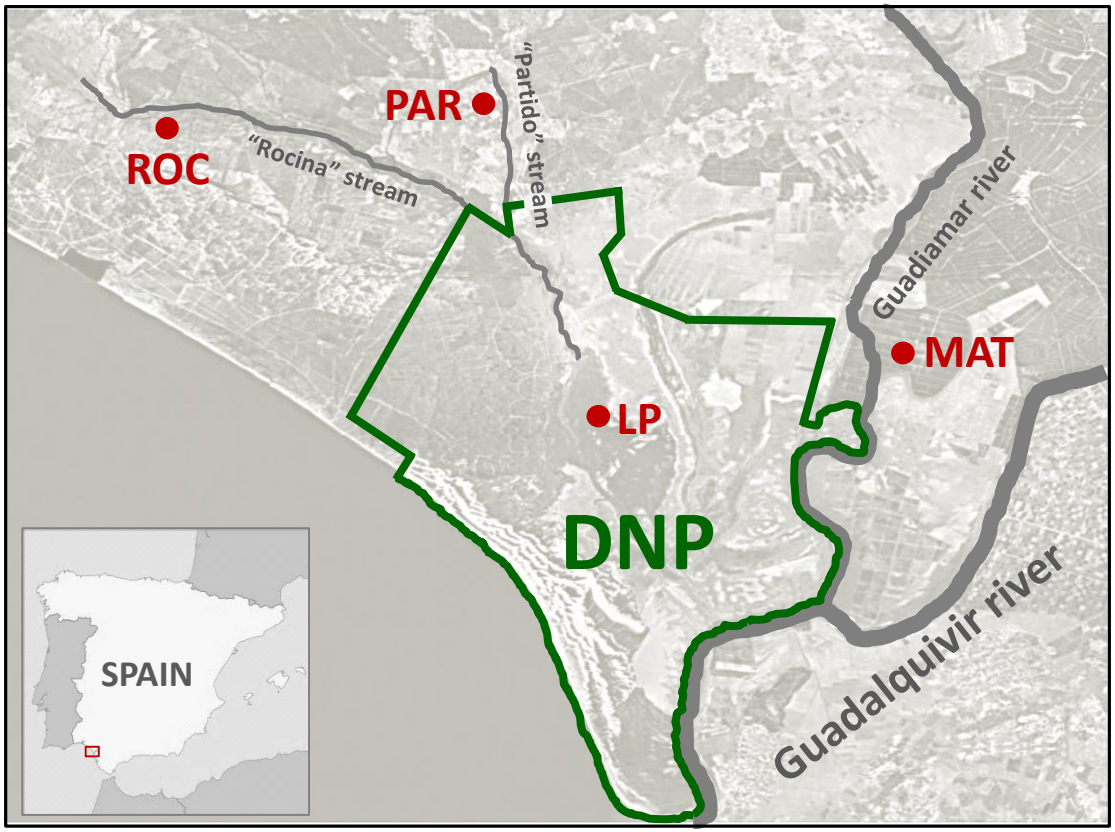

Site (code)	UTM coordinates	
Lucio del Palacio (LP)	*X = 189 947*	*Y = 4 098 578*
Matochal (MAT)	*X = 208 681*	*Y = 4 102 207*
Partido (PAR)	*X = 191 173*	*Y = 4 124 977*
Rocina (ROC)	*X = 178 653*	*Y = 4 119 937*

Figure 2

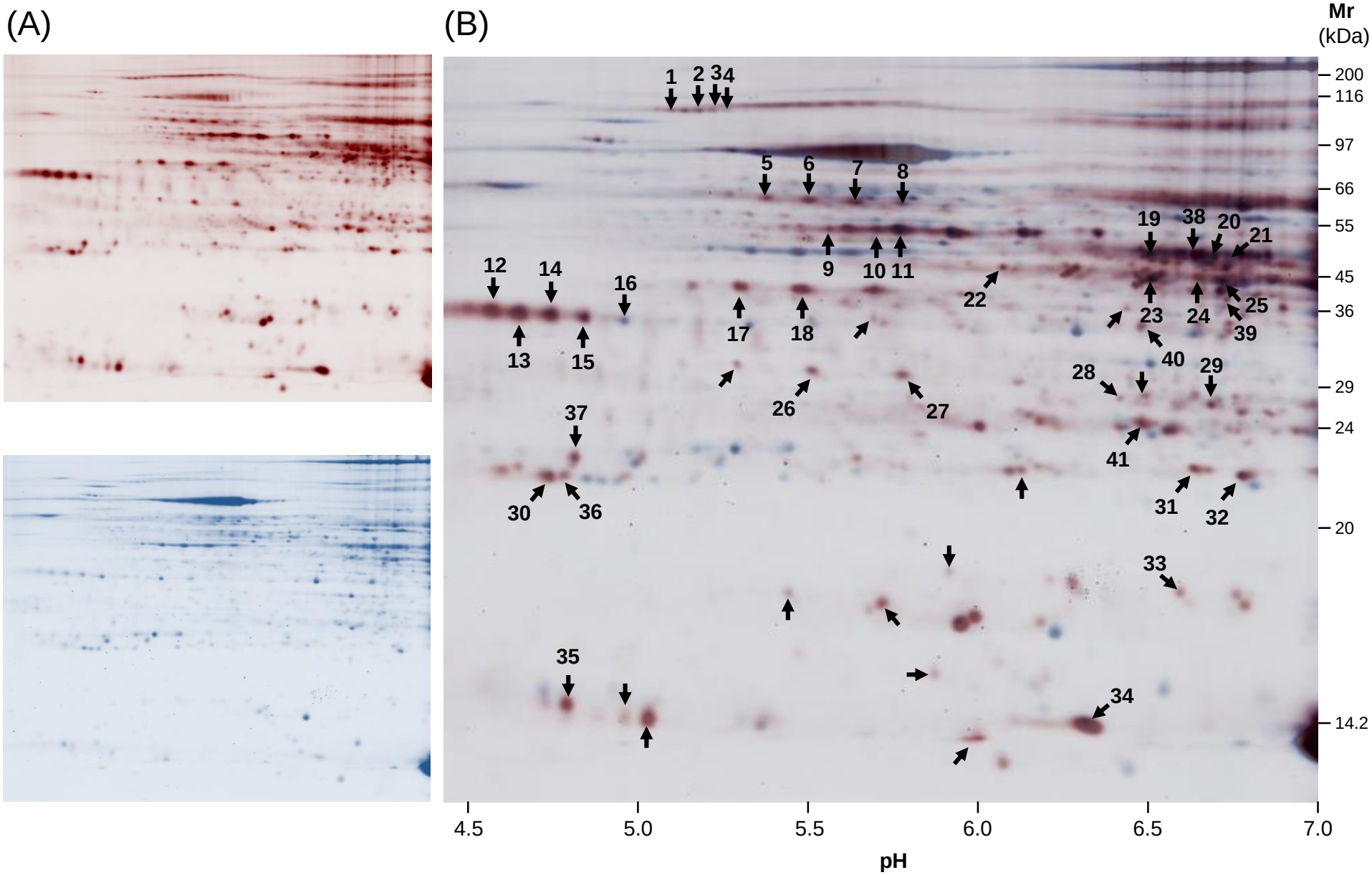
(A)
(B)
Mr
(kDa)
200
116
97
66
55
45
36
29
24
20
14.2
1
2
3
4
5
6
7
8
9
10
11
12
13
14
15
16
17
18
19
20
21
22
23
24
25
26
27
28
29
30
31
32
33
34
35
36
37
38
39
40
41
4.5
5.0
5.5
6.0
6.5
7.0
pH

Figure 3

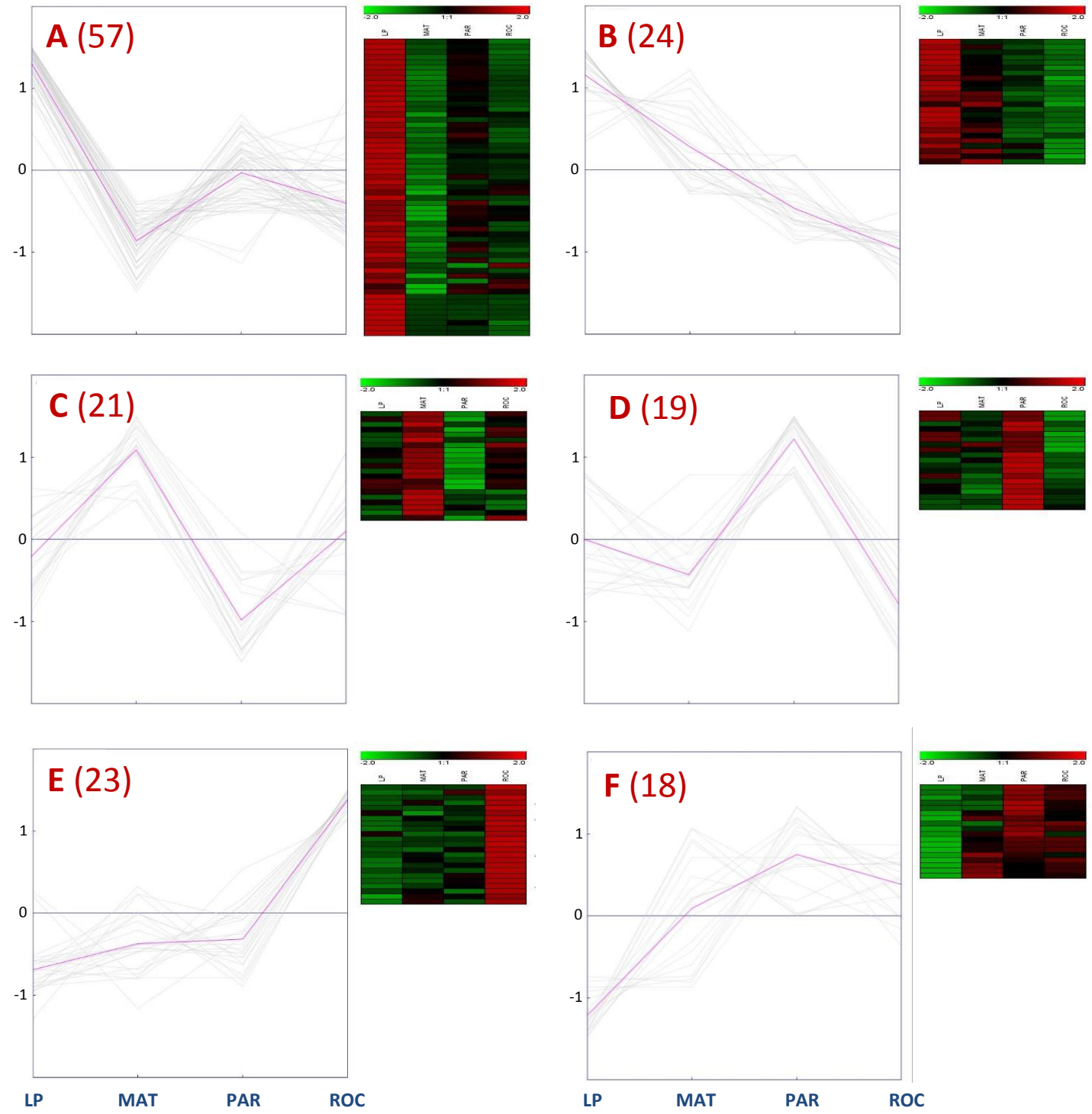

Figure 4

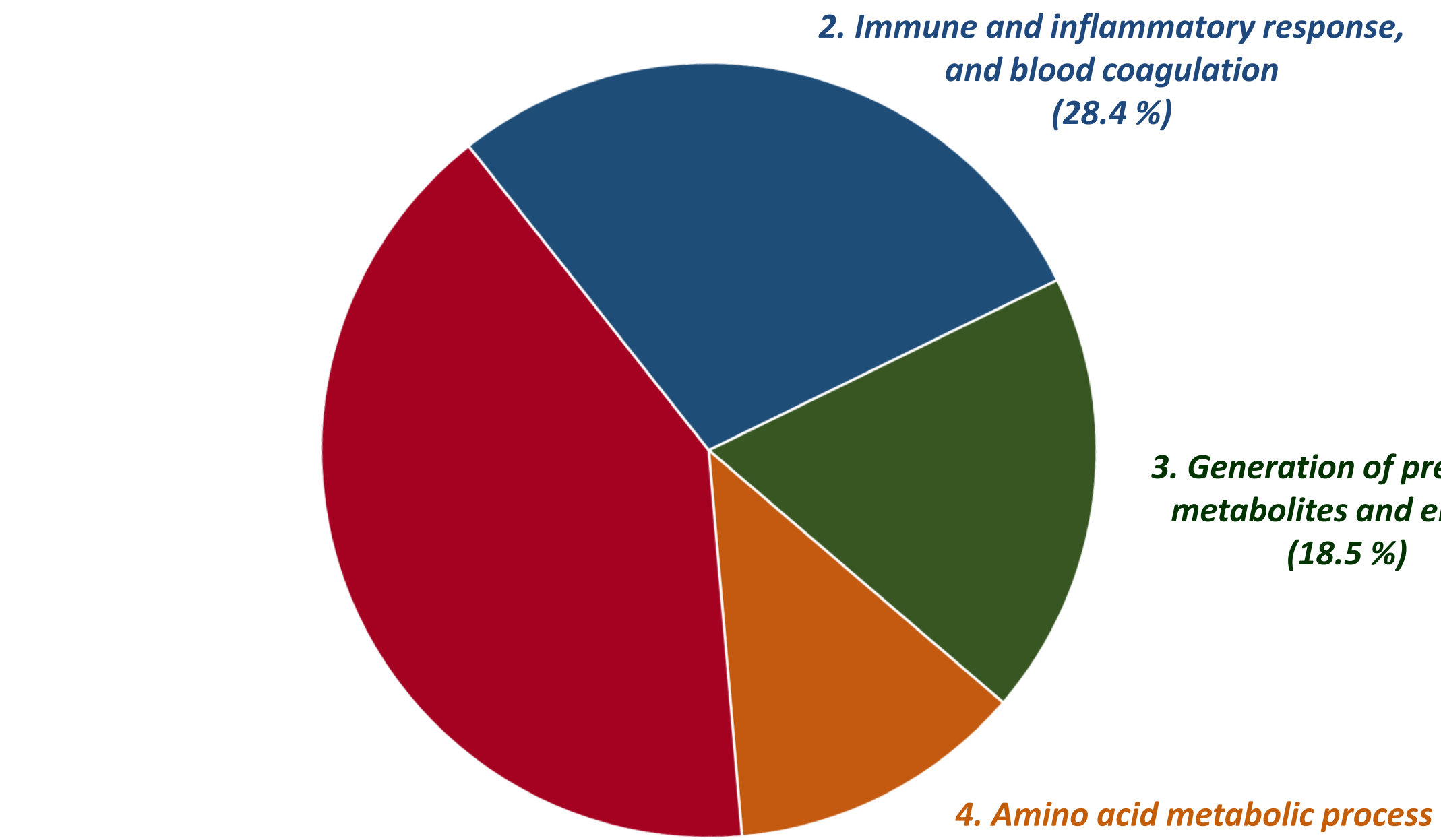
2. Immune and inflammatory response, and blood coagulation (28.4 %)
3. Generation of precursor metabolites and energy (18.5 %)
4. Amino acid metabolic process (12.3 %)
1. Cell redox homeostasis and detoxification (response to toxic substances and to oxidative stress) (40.7 %)

Figure 5

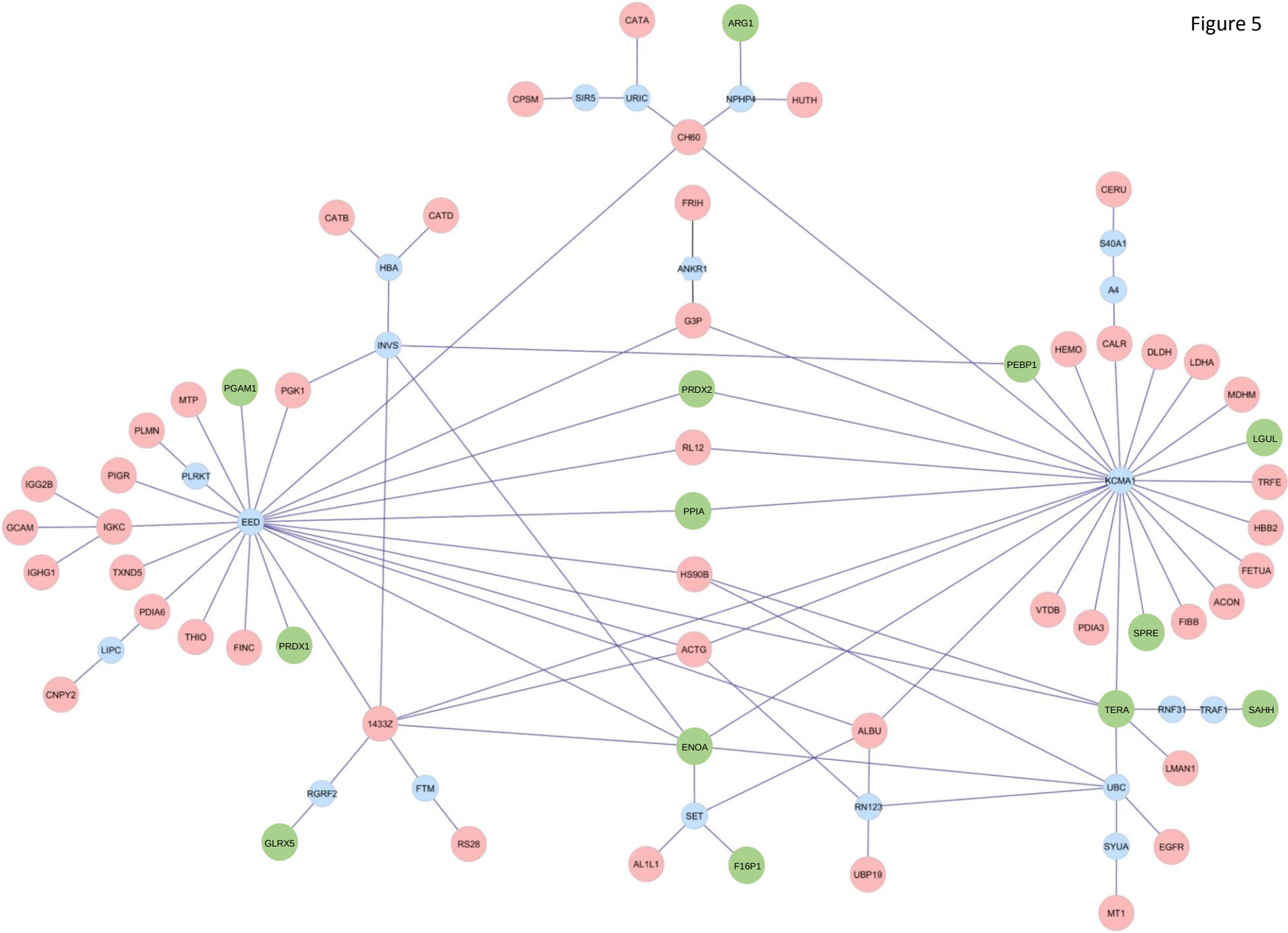
CATA
ARG1
CPSM
SIR5
URIC
NPHP4
HUTH
CH60
CERU
FRIH
S40A1
CATB
CATD
HBA
ANKR1
A4
G3P
CALR
INVS
HEMO
DLDH
LDHA
PEBP1
MDHM
PGAM1
PGK1
MTP
PRDX2
LGUL
PLMN
RL12
PIGR
PLRKT
KCMA1
TRFE
IGG2B
PPIA
GCAM
IGKC
EED
HBB2
IGHG1
TXND5
HS90B
FETUA
PDIA6
VTDB
ACON
PDIA3
SPRE
FIBB
THIO
FINC
PRDX1
LIPC
ACTG
CNPY2
TERA
RNF31
TRAF1
SAHH
1433Z
ALBU
ENOA
LMAN1
RGRF2
FTM
UBC
SET
RN123
SYUA
EGFR
GLRX5
RS28
AL1L1
F16P1
UBP19
MT1

Figure 6

(A)

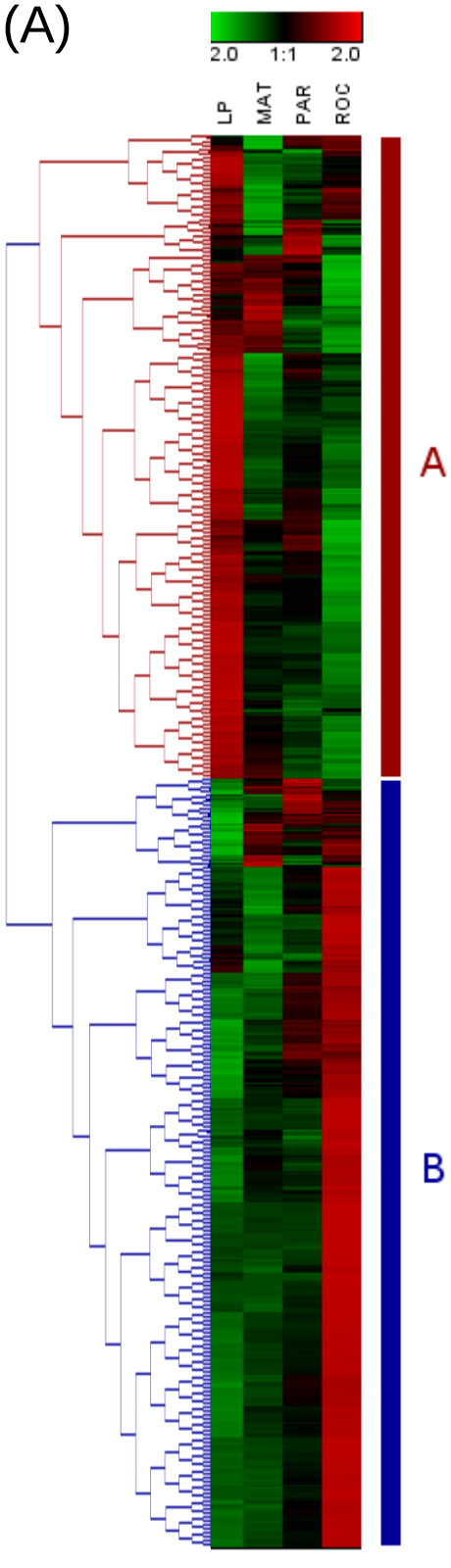

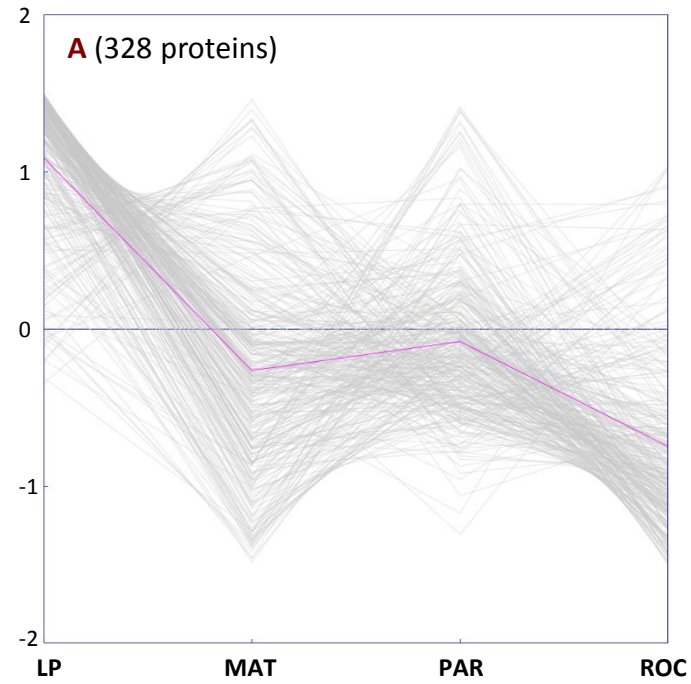

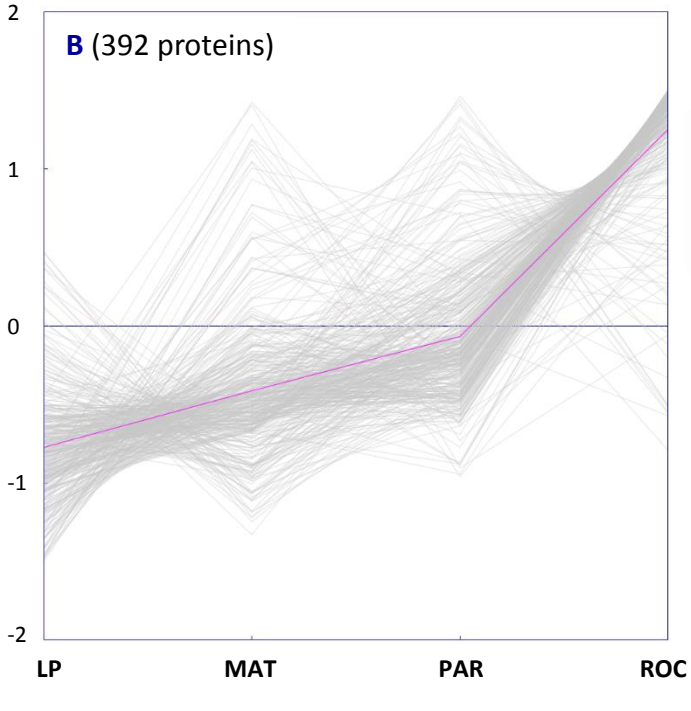

(B)

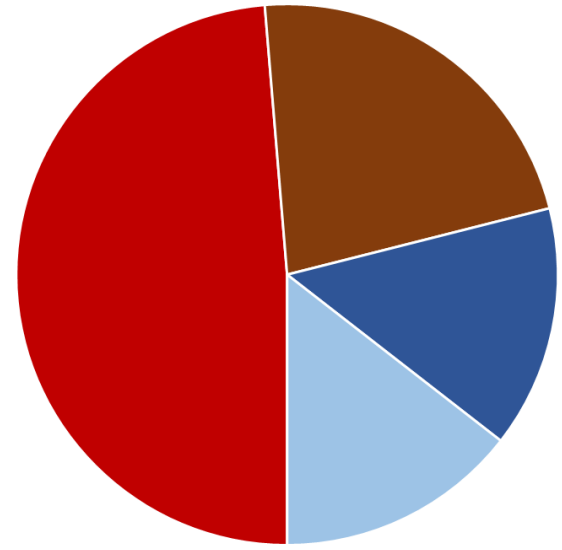

1. Biotransformation: drug/xenobiotic metabolism
2. Cholesterol biosynthesis and metabolism of steroids
3. Ubiquitin proteasome system activity and regulation
4. Amino acids metabolism (catabolism)

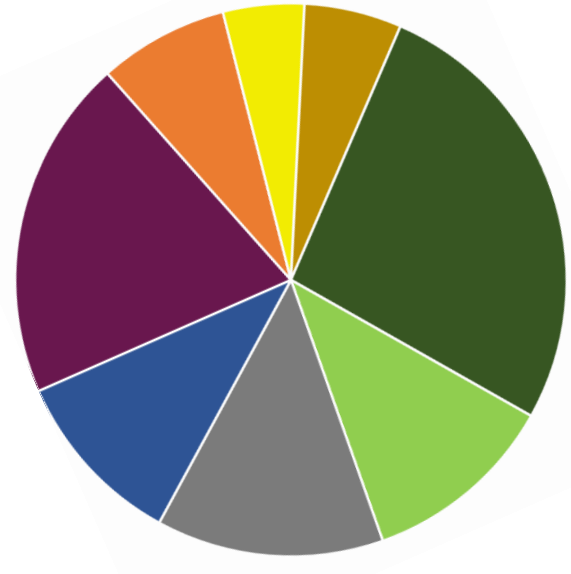

1. Response to oxidative stress and toxic substances
2. Fatty acid oxidation
3. Pyruvate metabolism
4. Electron transport chain and aerobic respiration
5. Structural constituent of ribosome involved in translation
6. Translation factors and cytoplasmic translation
7. Protein processing in ER and chaperonin-mediated folding
8. Ubiquitin proteasome system activity and regulation

HIGHLIGHTS

- Mice respond to toxic threats with changes in antioxidant/biotransformation enzymes, immune/inflammatory responses, and blood coagulation
- Most differentially oxidized proteins detected were involved in the maintenance of homeostasis
- Protein turnover was activated in response to oxidative damage to proteins, what demands a lot of energy
- Changes were detected in fatty acid oxidation and cholesterol metabolism
- The upregulation of biotransformation enzymes warns about organic pollution inside Doñana National Park